Fluid geochemistry and geothermometry in the western sector of the Sabatini Volcanic District and the Tolfa Mountains (Central Italy)

ARTICLE *in* CHEMICAL GEOLOGY · MARCH 2011

Impact Factor: 3.52 · DOI: 10.1016/j.chemgeo.2011.02.017

7 AUTHORS, INCLUDING:

Franco Tassi
University of Florence
385 PUBLICATIONS **1,842** CITATIONS
SEE PROFILE

Giordano Montegrossi
Italian National Research Council
97 PUBLICATIONS **615** CITATIONS
SEE PROFILE

Orlando Vaselli
University of Florence
425 PUBLICATIONS **3,141** CITATIONS
SEE PROFILE

F. Quattrocchi
National Institute of Geophysics and Volca…
64 PUBLICATIONS **437** CITATIONS
SEE PROFILE

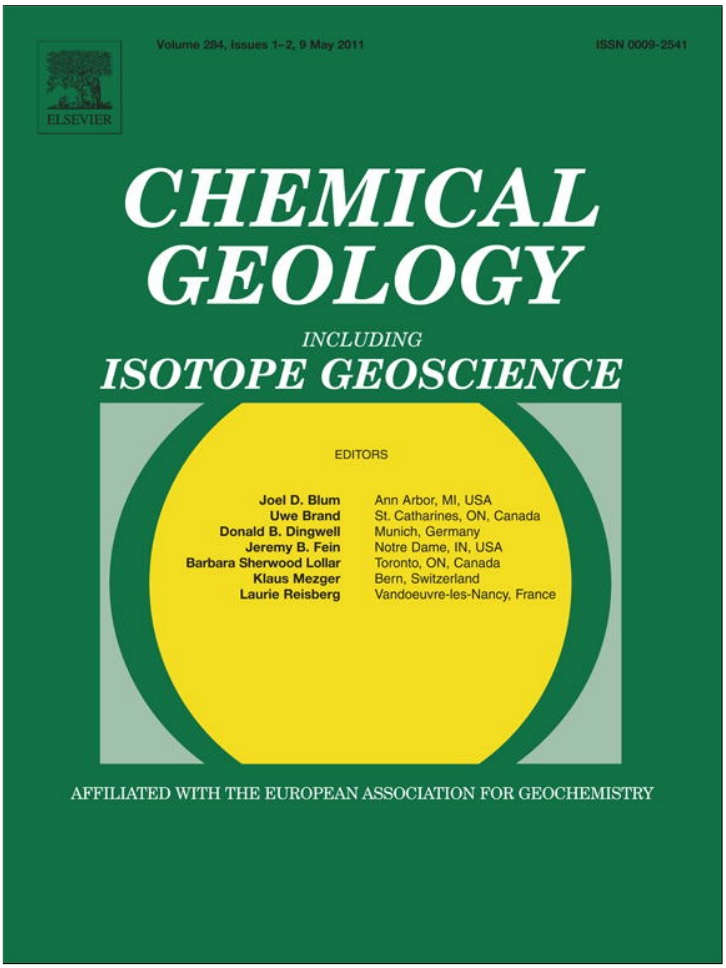

Chemical Geology 284 (2011) 160–181

Contents lists available at ScienceDirect

Chemical Geology

journal homepage: www.elsevier.com/locate/chemgeo

Fluid geochemistry and geothermometry in the western sector of the Sabatini Volcanic District and the Tolfa Mountains (Central Italy)

D. Cinti [a,*], M. Procesi [b], F. Tassi [c,d], G. Montegrossi [d], A. Sciarra [a], O. Vaselli [c,d], F. Quattrocchi [a]

[a] Istituto Nazionale di Geofisica e Vulcanologia (INGV), Via di Vigna Murata 605, 00143 Roma, Italy
[b] Dipartimento di Scienze Geologiche, Università di Roma Tre, Largo S. Murialdo 1, 00146 Roma, Italy
[c] Dipartimento di Scienze della Terra, Università di Firenze, via G. La Pira 4, 50121 Firenze, Italy
[d] CNR-IGG Istituto di Geoscienze e Scienze della Terra, via G. La Pira 4, 50121 Firenze, Italy

ARTICLE INFO

Article history:
Received 13 May 2010
Received in revised form 16 February 2011
Accepted 19 February 2011
Available online 26 February 2011

Editor: B. Sherwood Lollar

Keywords:
Geochemistry
Water
Gas
Stable isotope
Geothermometry
Central Italy

ABSTRACT

A geochemical survey of 197 fluid discharges (cold and thermal waters and bubbling pools) and 15 gas emissions from the western sector of the Sabatini Volcanic District and the Tolfa Mountains (Latium, Central Italy) was carried out in 2007–2008. The chemical and isotopic compositions of the fluid discharges indicate the occurrence of two main sources: 1) relatively shallow aquifers with Ca(Na,K)–HCO_3 and Ca(Mg)–HCO_3 compositions when trapped in volcanic and sedimentary formations, respectively; and 2) a deep reservoir, which is hosted in the Mesozoic carbonate sequence, rich in CO_2 and having a Ca–SO_4(HCO_3) composition. Dissolution of a CO_2-rich gas phase into the shallow aquifers produces high-TDS and high-pCO_2 cold waters, while oxidation of deep-derived H_2S to SO_4^{2-} generates low-pH (<4) sulfate waters.
The $\delta^{13}C$–CO_2 values for gas emissions (from −2.8 to +2.7‰ vs. VPDB) suggest that the origin of CO_2 associated with the deep fluids is mainly related to thermo-metamorphic reactions within the carbonate reservoir, although significant mantle contribution may also occur. However, R/R_a values (0.37–0.62) indicate that He is mainly produced by a crustal source, with a minor component from a crust-contaminated mantle. On the basis of the $\delta^{13}C$–CH_4 and δD–CH_4 values (from −25.7 to −19.5‰ vs. VPDB and from −152 to −93.4‰ vs. VSMOW, respectively) CH_4 production is associated with thermogenic processes, possibly related to abiogenic CO_2 reduction within the carbonate reservoir. The $\delta^{34}S$–H_2S values (from +9.3 to +10.4‰ vs. VCDT) are consistent with the hypothesis of a sedimentary source of sulfur from thermogenic reduction of Triassic sulfates. Geothermometric evaluations based on chemical equilibria CO_2–CH_4 and, separately, H_2S suggest that the reservoir equilibrium temperature is up to ~300 °C. The δD and $\delta^{18}O$ data indicate that water recharging both the shallow and deep aquifers has a meteoric origin. Fluid geochemistry, coupled with gravimetric data and tectonic lineaments, supports the idea that significant contributions from a deep-seated geothermal brine are present in the Stigliano thermal fluid discharges. Exploration surveys investigated this area during 70's–90's for geothermal purposes. Nevertheless, presently the area is still under-exploited. The presence of thermal waters and anomalous heat flow together with the demographic growth of the last years, makes this site a suitable location for direct applications of the geothermal resource.

1. Introduction

The Sabatini Volcanic District (SVD) and the Tolfa Mountains (TM) (Fig. 1) are part of the peri-Tyrrhenian sector of Central Italy, an area characterized by the presence of numerous thermal waters and CO_2-rich gas emissions (e.g. Baldi et al., 1973; Dall'Aglio et al., 1994; Duchi and Minissale, 1995; Chiodini et al., 1995, 1999; Minissale et al., 1997a,b; Minissale, 2004; Frondini et al., 2009). Thermalism in Central Italy is commonly attributed to the post-orogenic magmatic activity that occurred from Pliocene to Quaternary, in response to tectonic movements associated with the opening of the Tyrrhenian Sea. The origin of the main gas component (CO_2) has been ascribed to two different processes: 1) metamorphic decarbonation, and 2) mantle degassing (e.g. Minissale et al., 1997a and Frondini et al., 2009 and references therein).

Starting from late 1960s, geothermal prospection investigations in large areas of southern Tuscany and Latium (Larderello–Travale field, Mt. Amiata volcano, Latera–Torre Alfina and Cesano fields) were performed by ENEL (National Electric Energy Agency) and AGIP (National Oil Company) (Cataldi and Rendina, 1973; Bertrami et al., 1984; Carella et al., 1985; Cavarretta and Tecce, 1987; Barelli et al., 2000), in order to quantify the potential resources suitable for electricity generation. Temperatures exceeding 300 °C were measured in >3000 m

* Corresponding author. Tel./fax: +39 06 51860507.
E-mail address: daniele.cinti@ingv.it (D. Cinti).

0009-2541/$ – see front matter © 2011 Elsevier B.V. All rights reserved.
doi:10.1016/j.chemgeo.2011.02.017

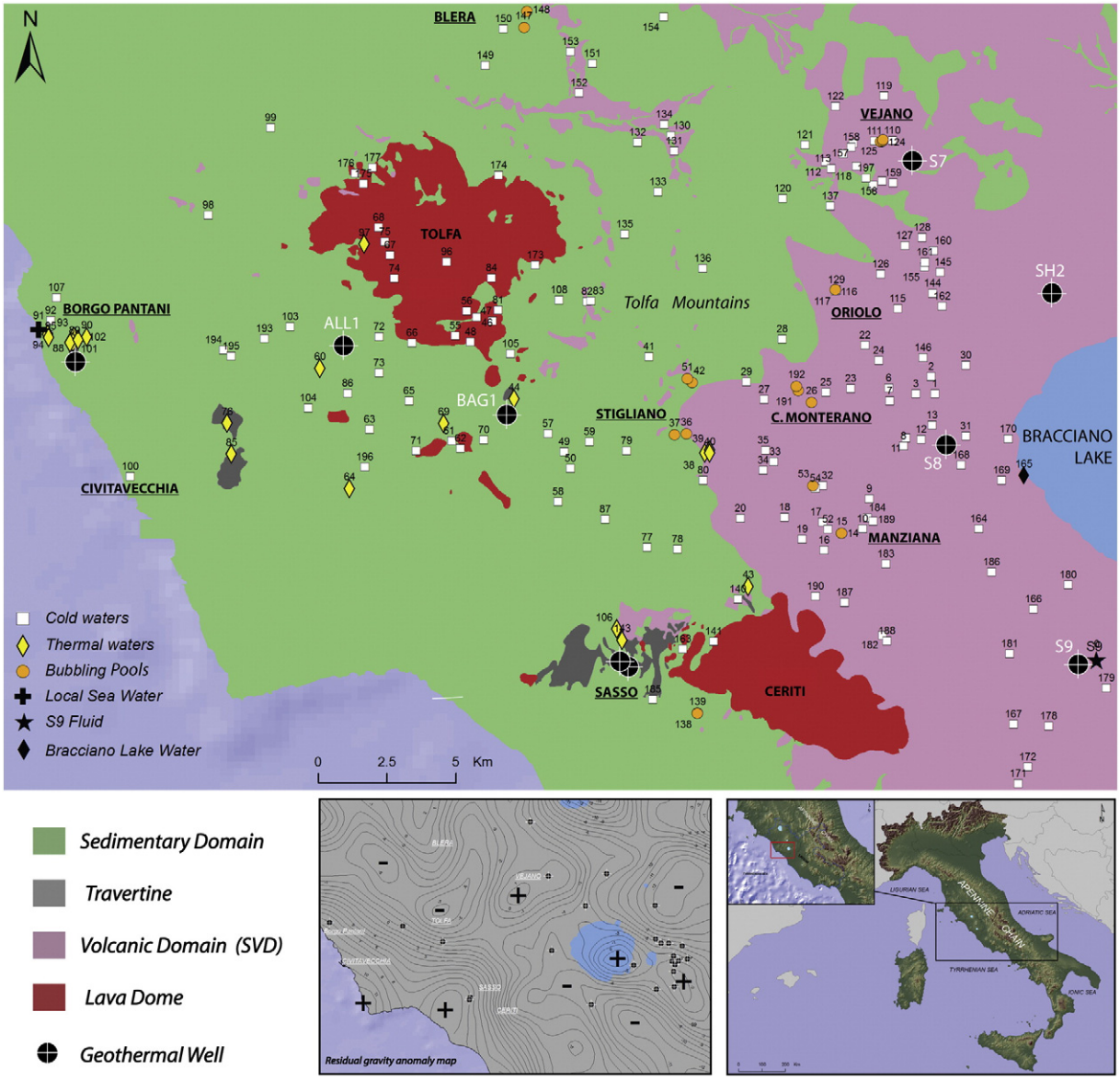

Fig. 1. Geological sketch map of the Sabatini Volcanic District (SVD) and the Tolfa Mountains (TM) showing the location of the fluid sampling sites and the main towns.

deep geothermal wells at Larderello, Mt. Amiata and Latera (Allegrini et al., 1995). During that period 24 deep wells and 61 test-holes were drilled in the SVD and TM, particularly in the Cesano area (eastern sector of the SVD; Fig. 1), where temperatures up to 220 °C were measured at a depth of about 1500 m in brines with TDS (Total Dissolved Solids) up to 350 g/L (Calamai et al., 1976; Funiciello et al., 1979; Barberi et al., 1994). In the western sector of the SVD and in the TM, where most of the thermal discharges and gas emissions are located, the maximum temperature (290 °C) was measured in the SH2 well, at a depth of about 2500 m (Cavarretta and Tecce, 1987). Despite the medium-to-high potential in terms of resources suitable for electricity generation (Allegrini et al., 1995), in the SVD and TM the attempts to produce electrical generation failed mainly due to the scaling problems during the exploitation.

In the present work a geochemical survey on thermal and cold waters and bubbling pools (197 samples) and associated gas phases (15 samples) discharging from the western sector of SVD and TM is presented to assess: 1) the fluid sources and the chemical–physical processes controlling the chemistry of the fluid discharges and 2) their relation to the structural setting of the area.

2. Geological, structural and hydrological settings

The study area extends from the western sector of the SVD to the town of Civitavecchia, along the Tyrrhenian margin of the Apennine chain (Fig. 1). This is part of the peri-Tyrrhenian sector of Central Italy, where during the Neogene a post-collisional extensional tectonic activity formed NNW–SSE oriented horst–graben structures and generated subduction-related magmatism (e.g. Barberi et al., 1994 and references therein). From W to E, two different geological domains can be recognized: 1) a sedimentary domain (Tolfa Flysch), constituted by silico-clastic turbiditic deposits and Plio-Pleistocene clays that crop out from TM to the Tyrrhenian Sea, and 2) a volcanic domain, formed by acid products of the Tuscan Magmatic Province and Quaternary undersaturated alkali–potassic volcanic rocks of the Roman Magmatic Province. The Tuscan volcanic products consist of rhyolites, rhyodacites and trachydacites that are found as dome complexes in the Tolfa (Tolfa Dome), Manziana and Sasso (Ceriti Dome) areas. The Roman volcanics, mainly consisting of pyroclastic and phreatomagmatic deposits, are centered on the Bracciano Lake and cover the entire

Table 1
Chemical and isotopic composition of water samples. Elevation in m; temperature (T) in °C; Eh in mV; pCO_2 in bar; $\delta^{18}O$ and δD as ‰ vs. VSMOW; total dissolved solids (TDS), F^-, Cl^-, Br^-, NO_3^-, SO_4^{2-}, HCO_3^-, Na, K, Mg, Ca, NH_4, Li, B, Sr, and SiO_2 in mg/L; s = spring; w = well; p = bubbling pool.

ID	Site	Type	X	Y	Depth	T	TDS	pH	Eh	pCO_2	F^-	Cl^-
1	Precilia	s	263583	4668977		15.5	234	6.55	233	0.017	0.21	15.6
2	Villa palombaro	s	263442	4669607		14.0	214	7.25	224	0.004	0.60	22.0
3	Via Oriolese	s	262888	4668976		17.8	291	7.17	217	0.008	0.10	23.0
6	Altare rupestre	s	261906	4669181		15.5	121	6.82	214	0.005	0.05	22.8
7	Quadroni	s	261941	4668723		17.1	334	6.81	210	0.019	0.23	21.9
8	Vivaio Motosi	w	262445	4667077	60	18.6	360	6.06	196	0.046	0.14	19.0
9	Ponte Mariano	w	261193	4665149	80	17.7	461	6.55	175	0.034	0.73	27.7
10	Ponte Mariano	w	260946	4664050	60	17.7	306	7.25	162	0.007	2.37	12.3
11	Casa dei Nonni	w	262531	4667363	65	17.1	599	5.56	158	0.125	1.40	12.4
12	Le Grazie	w	263077	4667320	70	17.7	366	5.59	191	0.067	0.31	13.5
13	Comune Manziana	w	263484	4667828	80	17.9	446	6.10	240	0.059	0.67	22.5
14	Caldara Manziana	p	260191	4663893		21.9	648	5.67	−230	0.119	2.26	13.7
15	Caldara Manziana	p	260191	4663893		25.8	2951	2.38	87	0	1.81	26.5
16	Fontanile Caldara	s	259545	4663278		17.2	299	6.88	105	0.014	1.13	14.3
17	Agriturismo Caldara	w	259498	4664303	60	18.0	286	6.99	117	0.011	1.13	15.3
18	Ferriere	s	258109	4664478		16.3	519	6.83	202	0.027	1.85	40.4
19	SP Aurelia–Braccianese	w	258745	4663677	45	17.4	195	6.63	213	0.012	0.30	10.1
20	Fosso Lenta	s	256499	4664435		17.5	762	5.52	144	0.159	1.66	13.8
22	Comune Canale M.	w	261036	4670740	65	17.1	238	6.79	160	0.014	0.99	10.3
23	Lavatoio	s	260515	4669173		16.5	269	6.83	90	0.014	0.17	23.4
24	Castel Donato	s	261530	4670182		14.2	162	6.25	152	0.018	0.03	17.2
25	Casa Merenda	w	259619	4669028	60	20.3	347	6.71	173	0.021	0.29	24.3
26	Parco di Diosilla	p	259087	4668656		27.0	550	4.07	−165	0.200	8.65	20.9
27	Fonte Rafanello	s	257368	4668771		20.0	1992	6.07	64	0.440	0.68	25.6
28	Fonte della Bandita	s	258013	4670976		22.6	738	7.43	145	0.016	0.10	23.1
29	Fonte del Castagno	p	256228	4670932		18.9	372	5.40	195	0.060	0.15	27.5
30	Comune Bracciano	w	264706	4670009	60	15.9	343	6.64	120	0.024	0.62	17.2
31	Sorgente Minciaro	s	264711	4667442		18.4	433	6.11	150	0.064	0.99	18.3
32	Ponton della Mola	w	259487	4665637	60	18.4	303	7.37	120	0.006	2.04	11.0
33	Prati di Canale	w	257712	4666505	80	19.2	502	6.52	150	0.047	2.24	22.0
34	Quarto Grande	w	257329	4666186	45	20.6	211	6.05	150	0.017	0.05	20.5
35	Acqua di Tito	s	257414	4666917		17.3	830	6.01	−200	0.145	1.52	16.2
36	Piana di Stigliano	p	254542	4667523		34.5	4704	6.31	−315	0.618	0.95	408
37	Piana di Stigliano	p	254104	4667492		26.7	4815	6.55	−260	0.380	1.17	441
38	Terme Stigliano	s	255212	4666805		51.9	4075	6.37	−315	0.441	2.45	141
39	Terme Stigliano	s	255379	4666908		24.2	4814	6.20	−295	0.651	2.22	355
40	Terme Stigliano	s	255381	4666809		38.0	4361	6.24	−266	0.584	1.97	193
41	Fontana Rota	s	253163	4670330		18.1	7956	6.43	34	0.903	1.05	220
42	Rota	p	254748	4669390		28.5	4371	6.51	−250	0.407	2.08	468
43	Casale Acquadoro	w	256786	4661948	103	40.3	3738	6.08	−155	0.281	2.23	27.4
44	Bagnarello	s	744183	4668514		46.1	3401	6.06	96	0.321	1.91	24.8
46	Fonte Limoiola	s	742605	4671394		14.3	447	5.90	170	0.007	0.04	96.7
47	Fonte Canale	s	743188	4671302		15.6	297	5.98	162	0.013	0.04	52.7
48	Fonte Lizera	s	742432	4670476		15.6	277	6.36	162	0.010	0.06	44.1
49	Sorgente della Nocchia	s	746133	4666723		17.5	691	7.17	123	0.023	<0.01	21.9
50	SP Tolfa–S.Severa	s	746396	4666140		20.0	814	7.45	107	0.016	<0.01	20.9
51	Polla Rota	p	254569	4669534		20.1	4588	6.16	−270	0.594	1.34	419
52	Caldara Manziana	w	259679	4664038	50	16.5	678	5.51	128	0.149	0.05	11.3
53	Via delle Fontanelle	p	259142	4665635		23.3	688	5.79	−110	0.111	2.00	14.3
54	Via delle Fontanelle	w	259230	4665527	60	18.6	294	6.60	99	0.021	0.56	17.0
55	Comune Tolfa	w	741877	4670676	100	15.3	136	4.61	105	0.002	0.12	20.4
56	Concia	w	742230	4671592	40	16.9	3186	6.71	−48	0.063	0.18	128
57	Fonte del Cerrobuco	s	745500	4667344		17.6	726	7.29	97	0.019	0.07	27.2
58	Fonte le Pantanelle	s	746026	4664895		18.5	667	7.87	85	0.005	<0.01	37.0
59	Fonte M. Castagno	s	747021	4667164		16.4	894	7.49	105	0.014	<0.01	51.6
60	Cesi della Vaccareccia	w	293669	4633809	110	23.5	866	7.00	205	0.043	0.46	54.9
61	Sorgente del Giglio	s	742022	4666833		18.4	412	6.81	198	0.022	0.04	38.0
62	Sorgente Fontanaccio	s	742355	4666583		18.0	464	7.34	159	0.008	0.08	46.1
63	Pontonaccio	s	738996	4667041		18.4	762	7.30	125	0.019	0.14	27.0
64	Maggiorana	w	738423	4664834	100	21.4	8157	6.47	11	0.980	0.80	111
65	Poggio della Stella	w	740370	4668176	80	17.4	1098	6.84	22	0.047	0.62	27.2
66	Fonte la Bianca	w	740311	4670302	65	17.0	103	4.86	210	0.004	0.11	32.8
67	Fonte del Connuto	s	739298	4673422		18.4	181	3.80	500	0.000	0.03	32.2
68	Acqua Acetosa	w	738816	4674400	80	19.3	3330	6.21	25	0.538	1.29	54.3
69	Poggio Selcioso	w	741686	4667442	100	23.5	1545	6.69	88	0.072	0.48	51.1
70	Fonte Granciare	s	743174	4666951		19.8	763	7.08	113	0.030	<0.01	33.1
71	Colle di Mezzo	w	740754	4666387	100	18.9	919	7.06	115	0.036	0.23	46.3
72	Fonte Porcareccia	s	739108	4670437		20.0	853	6.86	117	0.049	<0.01	32.6
73	Fonte Lappoleta	s	739198	4669121		24.1	802	7.83	113	0.005	0.09	25.9
74	Poggio Pinese	w	739516	4672580	40	17.4	395	6.85	126	0.018	0.04	31.9
75	Campaccio	w	739069	4673896	36	18.2	139	4.59	259	0.002	1.28	24.2
76	Terme Ficoncella	w	733813	4666904	42	51.1	2886	6.61	−155	0.156	1.72	22.4
77	Fonte dell'Olmo	s	253094	4663381		19.9	705	7.53	155	0.011	0.07	29.6
78	Fonte delle Cannucce	s	254216	4663305		18.0	698	7.52	140	0.011	<0.01	32.8

[a] Data from the S9 geothermal well are taken from unpublished ENEL reports.

Br^-	NO_3^-	SO_4^{2-}	HCO_3^-	Na	K	Mg	Ca	NH_4	Li	B	Sr	SiO_2	$\delta^{18}O$	δD	Elev.
0.12	6.09	8.65	116	20.6	12.6	5.68	16.4	<0.1	0.01	0.07	0.47	62.5			
0.11	0.49	6.68	97.6	23.1	17.6	4.27	10.4	<0.1	0.01	0.13	0.10	61.4	−6.7	−39	380
0.09	15.2	15.8	146	22.6	7.80	10.8	32.7	<0.1	0.01	0.17	0.33	31.7			
0.09	<0.01	8.11	45.8	17.8	2.82	3.68	6.87	<0.1	0.01	0.05	0.05	25.9			
0.05	9.39	16.9	183	20.4	9.89	12.8	34.8	<0.1	0.01	0.07	0.40	47.3			
0.12	0.04	59.6	170	17.3	14.4	16.4	39.6	<0.1	<0.01	0.05	0.38	47.0			
0.12	10.4	57.8	223	19.5	19.7	19.8	51.8	<0.1	0.01	0.05	0.29	59.9			
0.08	17.7	14.6	156	19.0	17.5	11.0	25.6	1.75	0.02	0.04	0.12	55.4			
0.13	6.64	21.7	372	12.7	24.6	13.7	88.7	<0.1	0.01	0.05	0.50	86.0	−6.5	−39	353
0.07	10.8	14.8	198	14.1	19.6	14.5	38.3	<0.1	0.01	0.10	0.48	81.8			
0.11	24.5	25.3	232	17.8	19.9	19.1	49.6	<0.1	<0.01	0.05	0.55	69.1			
0.66	<0.01	84.1	323	36.7	62.9	13.9	57.6	1.15	0.06	0.13	0.34	98.8	−10.6	−35	255
4.61	<0.01	2093	0	41.4	92.0	30.2	66.1	1.00	0.04	0.16	0.58	87.6	−0.8	−11	255
0.11	8.05	15.2	156	17.7	17.9	9.27	27.9	1.20	0.01	0.05	0.22	60.0			
0.06	10.8	15.8	149	14.2	10.1	9.04	33.3	1.00	0.01	0.04	0.09	51.4			
0.09	3.83	32.5	284	23.8	20.1	16.2	70.4	<0.1	0.02	0.05	0.33	51.3			
0.06	10.3	9.83	88.5	16.9	8.95	5.52	12.5	<0.1	<0.01	0.06	0.12	63.9			
0.38	0.27	35.1	464	50.3	50.5	12.9	78.3	1.00	0.05	0.22	0.59	96.5	−6.3	−37	190
0.08	12.6	5.23	128	14.5	8.20	9.28	23.5	<0.1	<0.01	0.05	0.33	49.3			
0.07	8.01	9.24	143	26.3	9.05	9.12	22.1	<0.1	0.01	0.15	0.19	34.1			
0.06	<0.01	7.18	85.4	17.4	2.56	4.43	15.9	<0.1	<0.01	0.03	0.10	23.9			
0.07	35.0	13.6	162	31.5	7.33	13.6	26.4	<0.1	0.02	0.25	0.21	65.1			
1.40	<0.01	349	0	32.7	20.1	6.76	29.0	<0.1	0.05	0.13	0.57	104	−9.2	−35	201
1.94	<0.01	41.9	1427	88.9	21.4	30.6	336	2.10	0.10	1.15	1.29	23.3	−5.9	−35	175
0.52	0.50	24.6	503	18.9	2.46	9.71	150	<0.1	<0.01	0.04	0.41	8.17			
0.03	11.1	37.0	163	26.8	16.1	9.56	38.4	<0.1	0.03	0.06	0.32	82.6			
0.07	18.0	12.8	180	21.8	24.5	11.0	29.3	<0.1	0.01	0.11	0.27	54.0			
0.08	9.78	12.0	247	21.5	28.1	15.0	41.1	<0.1	0.01	0.09	0.39	77.1			
0.08	4.65	11.2	178	14.2	13.6	8.66	35.8	<0.1	0.01	0.04	0.15	47.2			
0.06	16.7	20.3	284	29.8	23.8	12.5	60.5	<0.1	0.02	0.08	0.23	60.0			
0.12	5.38	40.2	58.0	12.8	13.9	6.94	18.1	<0.1	0.01	0.14	0.08	69.6			
<0.01	<0.01	31.3	540	62.7	28.1	15.9	96.0	<0.1	0.03	0.51	0.54	74.7	−6.4	−36	218
2.18	0.73	597	2306	501	72.8	77.1	532	104	1.79	76.2	9.26	29.6	−5.1	−40	140
1.76	<0.01	562	2322	571	90.9	61.8	552	103	3.09	74.5	8.72	39.8			
0.51	<0.01	1491	1318	197	30.8	131	692	24.0	0.97	23.6	9.81	25.9	−5.8	−38	150
1.32	<0.01	503	2599	453	65.9	68.7	585	84.0	2.86	68.4	8.70	33.2	−5.1	−40	155
0.82	<0.01	1098	1879	263	35.0	108	689	26.0	1.63	39.5	10.0	33.5	−5.6	−38	150
0.79	11.0	195	5368	1828	65.0	53.1	175	1.70	1.25	19.1	1.29	30.8	−5.8	−37	140
1.45	<0.01	302	2239	577	83.4	43.6	448	98.0	3.36	78.1	7.85	39.8	−5.6	−40	132
<0.01	4.47	2010	720	35.3	5.78	158	747	<0.1	0.09	2.90	12.2	25.7	−6.5	−37	246
<0.01	6.67	1737	720	41.5	11.6	125	700	<0.1	0.09	1.23	13.1	35.7	−6.5	−38	240
0.10	55.4	99.3	24.4	56.4	12.0	14.2	47.7	<0.1	0.06	0.90	0.49	78.8			
0.11	42.5	41.1	48.8	39.5	4.96	7.76	28.2	<0.1	0.03	0.23	0.20	62.1			
0.09	55.1	31.2	51.9	34.9	8.54	11.3	22.6	<0.1	0.01	0.26	0.28	32.9			
<0.01	12.9	21.8	461	17.8	1.16	7.91	142	<0.1	<0.01	0.16	0.61	8.47			
<0.01	9.97	23.0	555	16.0	1.07	3.98	178	<0.1	0.01	0.18	0.43	9.27	−6.3	−36	372
1.43	5.48	355	2471	511	69.9	63.1	490	104	3.28	73.8	7.37	23.2			
0.09	18.3	13.8	445	23.4	15.6	28.3	85.7	<0.1	0.01	1.04	0.68	67.9	−6.0	−36	268
0.00	<0.01	128	311	36.1	56.5	10.8	95.1	<0.1	0.04	0.47	0.80	62.1	−6.7	−37	265
0.06	22.3	16.7	140	14.8	11.2	10.9	31.8	<0.1	<0.01	0.21	0.18	55.5			
0.17	1.22	47.3	6.10	17.1	5.72	4.07	8.88	<0.1	<0.01	0.13	0.06	31.5	−7.1	−41	530
1.68	4.96	1618	598	126	9.62	240	438	<0.1	0.08	0.21	7.29	11.1			
<0.01	5.89	31.1	479	18.9	1.38	8.14	149	<0.1	0.01	0.21	0.55	8.67			
<0.01	5.31	16.1	433	25.5	1.11	4.06	140	<0.1	<0.01	0.07	0.43	9.46			
<0.01	29.3	33.6	561	46.4	7.22	31.7	130	<0.1	0.01	0.07	0.16	4.92			
<0.01	18.7	22.0	555	24.6	3.52	21.0	161	<0.1	0.02	0.09	1.83	6.93			
<0.01	13.6	33.4	207	26.1	22.7	9.89	54.6	<0.1	<0.01	0.04	0.08	11.5	−6.7	−35	450
<0.01	10.7	31.8	223	37.5	40.8	10.7	41.1	<0.1	<0.01	0.08	0.22	43.9			
<0.01	6.18	51.2	482	18.6	0.69	5.19	167	<0.1	<0.01	0.03	0.47	7.23			
<0.01	49.8	87.5	5734	2044	15.1	22.4	78.0	0.70	0.25	2.12	1.78	18.5	−6.1	−32	285
<0.01	4.83	285	506	14.8	1.48	35.9	218	<0.1	<0.01	0.04	0.41	4.43	−6.6	−36	480
<0.01	4.05	19.4	10.4	21.5	2.82	3.67	3.96	<0.1	<0.01	0.03	0.07	8.09			
<0.01	0.72	65.1	0	27.9	12.2	4.89	4.98	<0.1	<0.01	0.03	0.05	59.7			
<0.01	6.49	64.4	2410	69.2	23.5	90.7	593	4.61	0.17	0.23	5.45	10.9	−7.0	−38	210
<0.01	2.43	530	555	40.4	3.13	79.2	250	<0.1	0.02	0.04	16.6	33.1	−6.6	−35	435
<0.01	4.26	59.4	476	18.4	0.82	14.3	152	<0.1	<0.01	0.03	0.30	7.64			
<0.01	3.76	70.6	567	35.3	2.36	29.0	157	<0.1	0.03	0.05	2.13	10.3			
<0.01	12.4	73.6	519	19.4	0.59	8.63	183	<0.1	<0.01	0.03	0.33	7.96			
<0.01	4.57	166	397	19.4	0.21	10.2	174	<0.1	<0.01	0.03	0.36	7.97			
<0.01	1.71	40.4	192	28.2	7.43	3.66	61.8	<0.1	<0.01	0.03	0.11	54.1			
<0.01	0.51	38.8	6.10	23.4	6.83	2.97	2.99	<0.1	0.03	0.03	0.03	61.6			
<0.01	5.75	1415	677	41.3	4.90	94.0	594	<0.1	0.03	0.12	12.5	32.7	−6.7	−37	180
<0.01	4.82	34.9	464	20.8	0.53	23.1	122	<0.1	<0.01	0.04	0.52	9.36			
<0.01	7.94	25.6	458	19.5	0.82	16.1	133	<0.1	<0.01	0.03	0.53	7.28			

(continued on next page)

Table 1 (*continued*)

ID	Site	Type	X	Y	Depth	T	TDS	pH	Eh	pCO_2	F^-	Cl^-
79	Fonte valle Giuncosa	s	252353	4666894		20.3	637	7.31	130	0.017	0.08	16.9
80	Fonte Capannone	s	255140	4665819		18.0	314	6.86	150	0.015	0.03	18.3
81	Fontana Guarente	s	743359	4671706		21.3	179	7.32	125	0.002	0.04	24.9
82	Pian Cisterna	w	746562	4672248	20	18.0	615	7.04	165	0.020	<0.01	34.4
83	Pisciarello di S. Biagio	s	746714	4672277		24.8	564	7.30	154	0.015	0.09	30.3
84	Poggio Casalavio	s	743039	4672850		20.5	316	6.25	23	0.026	0.14	48.0
85	Civitavecchia 1	w	734060	4665791		46.1	2920	6.13	−142	0.303	1.61	23.1
86	Fontanile Miniera	s	738120	4668307		19.2	983	7.09	40	0.027	0.21	32.2
87	Fonte le Catenare	s	747784	4664378		16.9	801	6.93	205	0.045	<0.01	21.7
88	Albani & Ruggeri 1	w	728038	4669662	320	39.7	4761	6.17	−280	0.664	1.65	482
89	Albani & Ruggeri 2	w	728008	4669453	320	40.9	4927	6.18	−286	0.684	1.74	546
90	Albani & Ruggeri 3	w	728500	4669680	320	47.3	5053	6.26	−292	0.703	1.65	569
92	La Frasca	w	727142	4670192	50	18.7	1328	7.16	43	0.024	<0.01	219
93	La Frasca	w	727084	4669672	63	20.8	1457	6.63	−106	0.086	0.54	147
94	La Frasca	w	727109	4669659	40	19.2	2096	6.44	−70	0.157	0.20	260
95	La Frasca	w	727115	4669553	40	22.1	3370	6.60	62	0.147	0.46	396
96	Campacceto	w	741369	4673329	26	15.3	511	7.19	95	0.015	0.63	18.8
97	Monte Rovello	w	738339	4673748	95	20.4	2957	6.11	−5	0.494	0.23	142
98	Pian dell'Organo	w	732595	4674401	25	19.0	853	7.37	−120	0.013	0.28	58.2
99	Campo di Marte	w	734630	4677749	40	19.7	1672	7.28	44	0.027	0.54	325
100	Civitavecchia	w	730433	4664728	45	18.3	876	7.23	59	0.018	0.08	73.1
101	Albani & Ruggeri 4	w	727910	4669423	320	37.7	4456	6.25	−280	0.581	1.97	479
102	Albani & Ruggeri 5	w	728198	4669551	320	36.7	4605	6.29	−280	0.551	1.73	490
103	Fonte Pocopane	s	735856	4670566		15.2	755	7.91	80	0.005	<0.01	10.9
104	Tramontana	w	736709	4667666	80	17.8	1204	7.00	−6	0.036	0.53	197
105	Casale dei Frati	w	743922	4670157	25	15.4	954	6.96	−2	0.033	0.19	142
106	Dolomiti del Lazio	w	252004	4660398	57	35.6	3240	6.05	−105	0.240	1.69	30.8
107	Albani & Ruggeri 6	w	727297	4671029	50	17.6	1604	7.05	88	0.021	0.13	91.3
108	Pian Cisterna	w	745549	4672228	50	17.1	1119	8.37	−107	0.002	3.28	72.6
109	Caldara Vejano	p	261638	4678152		12.6	396	5.35	−120	0.068	0.67	18.1
110	Fonte Streppaie	s	262045	4678198		12.2	178	6.43	80	0.011	1.00	10.8
111	Acqua Forte	s	261388	4678184		14.4	558	5.50	76	0.112	0.54	17.8
112	Fontanile Sodi	s	259603	4677407		13.5	287	6.99	110	0.009	0.27	20.2
113	Fonte Vigna Grande	s	259812	4677169		9.3	182	7.45	106	0.002	0.26	13.1
114	Fonte Vejano	s	260235	4677711		15.0	408	7.44	105	0.003	0.23	43.2
115	Fonte Serrale	s	262222	4672077		12.8	118	7.10	98	0.003	0.08	5.27
116	Parco della Mola	p	259956	4672768		27.4	742	5.66	−194	0.198	0.63	11.9
117	Fonte Parco d. Mola	s	259960	4672720		11.7	274	6.63	70	0.018	0.76	11.0
118	Fonte M. Gennaro	s	260717	4677252		11.5	187	7.96	64	0.001	0.70	13.2
119	Fonte le Pantane	s	261722	4679826		11.9	178	7.38	89	0.003	0.10	11.0
120	Fonte M. Casella	s	258044	4676081		12.2	580	7.54	64	0.009	0.06	14.7
121	Pastinello	w	258857	4678041	60	12.8	861	7.15	−44	0.026	0.44	36.1
122	Comune Vejano	w	259953	4679441	35	13.0	313	6.92	50	0.014	0.36	13.0
123	Caldara Vejano	p	261610	4678152		7.2	383	5.58	−72	0.047	0.20	15.7
124	Caldara Vejano	p	261682	4678178		7.9	360	5.16	−163	0.049	0.28	13.5
125	Caldara Vejano	p	261700	4678223		11.9	173	4.15	−55	0	0.05	17.8
126	Fonte Pascolaro	s	261607	4673317		11.3	170	7.08	135	0.005	0.04	11.6
127	Fonte Cacapece	s	262495	4674372		11.3	211	6.79	140	0.009	0.11	15.4
128	Fonte Piscinello	s	263107	4674662		9.3	193	7.39	120	0.003	0.07	12.5
129	Fonte Parco d. Mola	s	259999	4672746		13.2	384	5.04	−105	0.045	0.44	9.15
130	Civitella di Cesi	s	253971	4678375		10.0	312	7.37	6	0.003	0.34	29.1
131	Fonte delle 3 Vasche	s	254082	4677811		14.8	512	7.63	26	0.004	0.53	24.8
132	Fonte di Cammerata	s	252760	4678124		13.0	810	7.01	57	0.033	0.18	54.1
133	Fonte Vaccarecce	s	253503	4676321		11.2	548	7.74	60	0.005	<0.01	10.9
134	Fonte Lontaneto	s	253722	4678779		15.0	293	6.96	190	0.009	0.86	14.6
135	Ponton d. Sorca	w	252283	4674777	4	10.6	658	6.80	160	0.040	0.13	18.8
136	Vacchereccia	w	255131	4673529	45	19.8	907	6.87	−2	0.053	0.20	55.5
137	Valle Campane	w	259765	4675794	60	16.0	691	7.09	202	0.029	0.24	14.1
138	M. Solferata	p	254931	4657354		11.1	15168	3.92	−145	0.610	16.5	63.8
139	M. Solferata	p	254928	4657332		8.9	9353	1.57	70	0.890	2.69	72.3
140	Fonte Fumarolo	s	256406	4661497		15.3	341	6.61	40	0.025	0.17	23.2
141	Fonte Sasso	s	255522	4659950		12.8	349	6.99	40	0.011	0.06	52.1
142	Villa d'Este	w	261326	4676564	35	11.9	262	6.51	100	0.021	0.24	18.1
143	Pian d. Carlotta	w	252190	4659989	35	36.1	3323	6.04	170	0.234	1.35	28.7
144	Oriolo	w	263495	4672635	45	9.3	234	7.16	55	0.006	0.30	11.8
145	Strada Fontanella	w	263774	4673387	115	14.1	186	7.22	95	0.004	0.14	8.10
146	Vivaio M. Virginio	w	263143	4670296	110	15.3	587	6.36	120	0.072	0.12	10.1
147	Poggio del Fattore	w	743592	4682041	60	16.6	5802	6.34	46	0.678	<0.01	206
148	Poggio Saracino	w	743651	4682631	60	19.8	5244	6.33	−100	0.656	<0.01	182
149	Acqua Acetosa	s	742271	4680560		11.8	3995	6.74	30	0.232	<0.01	181
150	Fonte Murata	s	742838	4681943		13.2	1072	6.96	60	0.045	0.11	80.3
151	Fonte Vergine	s	746148	4680904		11.3	819	7.10	66	0.027	0.12	38.7
152	Fonte Sambuco	s	745746	4679804		14.4	364	7.06	160	0.007	1.10	16.5
153	Fonte la Casentile	s	745318	4681279		12.8	620	7.37	130	0.006	0.27	39.1
154	Fonte dei Trocchi	s	253708	4682697		13.5	808	7.02	110	0.028	0.17	55.3
155	Via Santo Ianni	w	263195	4673581	60	12.9	197	7.58	110	0.002	0.13	11.7

Br^-	NO_3^-	SO_4^{2-}	HCO_3^-	Na	K	Mg	Ca	NH_4	Li	B	Sr	SiO_2	$\delta^{18}O$	δD	Elev.
<0.01	10.8	22.6	427	11.5	0.39	8.17	133	<0.1	<0.01	0.05	0.47	12.1			
<0.01	16.9	12.9	156	17.5	22.4	6.12	34.2	<0.1	0.01	0.19	0.35	59.3			
<0.01	11.0	22.2	54.9	21.7	2.16	4.39	17.7	<0.1	0.01	0.04	0.11	40.2			
<0.01	60.8	22.7	305	26.3	22.6	5.53	104	4.78	0.01	0.07	0.41	55.3			
<0.01	17.0	17.9	331	34.1	14.1	9.08	80.8	<0.1	0.01	0.08	0.45	59.0	−6.1	−34	205
<0.01	0.37	30.8	107	44.2	12.1	6.45	17.7	<0.1	0.03	0.09	0.11	95.3			
<0.01	6.92	1397	726	44.7	4.61	95.6	598	<0.1	0.04	0.12	10.7	23.3			
<0.01	4.14	238	458	22.5	1.65	32.1	187	<0.1	0.01	0.03	0.32	11.4			
<0.01	4.72	12.5	565	17.9	1.09	9.69	163	<0.1	0.01	0.06	0.61	9.59			
0.76	2.79	1011	1903	471	58.9	80.6	681	3.30	3.69	35.3	9.61	28.0			
0.15	6.85	1011	1946	496	56.4	88.4	702	3.20	4.07	40.2	10.4	27.1			
0.71	4.61	1035	1976	505	59.6	93.4	730	3.70	4.26	43.7	10.8	28.4	−6.3	−36	36
<0.01	12.7	226	470	211	3.31	38.6	140	<0.1	0.02	0.82	0.85	11.8			
0.14	2.07	250	622	219	14.4	35.8	141	9.60	0.47	5.80	2.00	12.3			
<0.01	3.48	311	909	215	20.2	66.3	279	2.30	0.92	11.2	3.71	17.6			
1.13	71.3	835	1043	375	53.6	75.7	467	<0.1	2.82	28.8	6.85	25.2			
<0.01	12.3	15.0	317	25.7	3.13	6.52	94.6	<0.1	0.03	0.52	0.23	33.3			
<0.01	2.58	93.0	1928	286	19.8	61.3	407	<0.1	0.36	0.93	4.66	15.1			
<0.01	3.89	160	384	64.4	31.4	25.1	115	<0.1	0.01	0.44	0.96	11.5			
<0.01	8.70	141	671	367	15.9	44.8	86.4	<0.1	0.18	2.38	1.32	13.5			
<0.01	36.8	126	409	86.0	6.80	35.2	95.3	<0.1	0.03	0.59	0.54	13.7			
1.89	17.2	797	1897	443	50.6	79.3	618	3.20	3.94	37.5	12.4	27.1			
<0.01	17.5	850	1934	456	55.6	82.5	644	3.30	3.96	38.6	12.6	27.4			
0.26	4.04	64.2	473	30.7	1.38	13.1	151	<0.1	<0.01	0.47	1.08	11.9			
<0.01	4.11	154	525	84.8	13.6	68.7	140	<0.1	0.14	0.59	9.46	11.4			
0.25	19.8	48.5	451	172	3.69	19.0	81.0	<0.1	0.03	0.30	0.88	29.8			
1.04	9.64	1705	647	41.1	6.71	139	629	1.00	0.08	0.66	11.6	29.0	−6.6	−35	265
<0.01	20.7	699	348	88.5	7.84	45.6	292	2.16	0.01	0.25	2.19	15.2			
<0.01	2.14	38.7	671	312	5.43	1.55	3.02	<0.1	0.05	4.09	0.23	10.0			
0.05	1.39	7.99	220	24.1	22.2	6.71	44.1	1.20	0.04	0.20	0.46	95.1	−10.3	−35	350
0.06	9.32	9.85	64.1	19.9	17.1	1.35	8.48	<0.1	0.01	0.07	0.05	71.1			
<0.01	2.67	0.52	354	27.4	16.7	11.9	75.0	1.10	0.03	0.13	0.63	89.5	−6.5	−36	350
<0.01	8.52	16.7	134	21.1	14.7	8.21	26.2	<0.1	0.01	0.08	0.20	72.9			
<0.01	5.18	15.8	67.1	21.3	16.4	1.97	7.97	1.50	<0.01	0.05	0.04	63.1			
<0.01	82.1	30.0	110	32.6	27.8	12.1	37.1	<0.1	<0.01	0.10	0.19	64.9			
<0.01	15.2	2.40	51.9	9.54	1.70	4.72	9.90	<0.1	<0.01	0.05	0.16	34.8			
<0.01	0.77	20.8	470	53.6	38.6	17.1	65.4	3.50	0.05	0.22	0.35	118	−7.6	−36	300
<0.01	5.74	4.40	146	17.6	21.1	7.24	22.5	<0.1	0.01	0.07	0.23	72.5			
<0.01	5.45	6.79	79.3	19.6	16.4	2.92	9.12	<0.1	0.02	0.06	0.07	66.0			
<0.01	7.16	3.75	85.4	13.1	2.99	5.67	17.1	<0.1	<0.01	0.05	0.20	63.4			
<0.01	1.10	18.9	390	15.2	3.29	6.28	125	<0.1	<0.01	0.05	0.51	8.70			
<0.01	1.57	64.3	537	79.5	3.39	52.5	72.1	3.00	0.04	0.30	0.60	19.2	−6.2	−34	425
<0.01	5.30	10.1	174	21.8	17.6	7.37	31.4	<0.1	0.01	0.08	0.25	63.6			
<0.01	3.26	44.2	192	30.2	13.7	11.2	40.6	1.05	<0.01	0.10	0.59	55.1			
<0.01	1.62	27.6	180	20.3	16.4	7.09	41.5	1.02	0.04	0.09	0.43	95.5	−13.3	−35	350
<0.01	0.42	74.0	0	14.3	8.49	4.98	14.1	1.10	<0.01	0.04	0.61	62.3	−6.9	−36	350
<0.01	0.68	2.46	82.4	12.0	9.46	4.25	12.3	<0.1	<0.01	0.06	0.18	69.2			
<0.01	14.3	7.30	94.6	12.8	6.30	8.25	21.5	<0.1	<0.01	0.03	0.44	60.6			
<0.01	5.30	5.79	101	10.5	4.62	7.79	19.6	<0.1	<0.01	0.03	0.23	52.4			
<0.01	2.00	92.1	137	24.3	26.7	12.3	31.1	1.70	0.02	0.07	0.70	70.6	−6.9	−36	300
<0.01	30.9	23.8	110	39.1	14.8	5.55	23.0	<0.1	0.01	0.09	0.19	70.3			
<0.01	57.1	24.2	235	34.9	25.2	8.11	69.0	<0.1	0.01	0.10	0.23	65.0			
<0.01	3.07	23.0	509	46.0	1.01	11.1	155	<0.1	<0.01	0.07	0.57	12.1			
<0.01	5.22	12.4	381	11.2	0.89	5.27	115	<0.1	<0.01	0.06	0.34	9.46			
<0.01	26.5	20.5	116	33.4	19.9	2.99	21.9	<0.1	0.02	0.09	0.13	72.8			
<0.01	2.43	31.0	439	23.8	0.51	8.62	128	<0.1	<0.01	0.08	0.42	10.0			
<0.01	1.77	40.9	576	33.9	3.63	26.6	160	<0.1	0.02	0.08	0.71	13.4	−6.1	−35	278
<0.01	1.55	8.35	494	14.9	1.73	6.46	142	1.05	<0.01	0.04	0.52	11.9			
1.31	163	11405	0	71.4	25.5	251	391	0.50	0.51	0.73	2.75	95.7	−16.3	−15	80
<0.01	163	7935	0	58.2	21.9	59.3	374	0.50	0.19	0.67	1.96	140	−14.5	−22	80
0.09	13.1	11.5	183	26.2	6.06	11.1	35.2	<0.1	0.01	0.08	0.39	61.4			
0.09	11.7	19.4	153	39.6	18.7	12.1	24.8	<0.1	0.01	0.06	0.27	34.5			
0.02	1.89	7.57	146	23.5	19.4	5.95	20.3	<0.1	0.01	0.10	0.38	32.7			
<0.01	166	1645	622	36.6	6.65	142	642	3.60	0.07	0.47	12.7	30.7	−6.5	−36	250
<0.01	16.9	5.15	122	13.0	8.47	9.63	21.1	<0.1	<0.01	0.04	0.38	50.6			
<0.01	25.3	2.91	85.4	10.0	7.02	7.39	16.5	<0.1	<0.01	0.03	0.18	46.3			
0.06	14.0	2.64	387	23.5	25.0	21.1	64.7	<0.1	<0.01	0.06	0.45	76.3			
<0.01	16.1	278	3752	756	99.3	106	537	11.0	2.01	11.5	12.8	28.4			
<0.01	166	185	3355	601	95.1	106	512	10.0	1.64	10.3	9.73	15.9	−8.6	−40	210
<0.01	23.4	230	2471	571	42.4	83.7	377	6.00	0.54	4.60	2.51	5.96	−6.1	−38	160
<0.01	12.9	46.9	653	45.5	2.33	20.9	203	<0.1	<0.01	0.08	0.57	14.6			
<0.01	24.3	37.9	506	20.6	0.42	5.67	178	<0.1	<0.01	0.05	0.50	12.9			
0.04	85.1	28.3	113	32.0	21.7	7.55	31.2	<0.1	0.01	0.08	0.13	54.5			
<0.01	173	21.5	201	39.2	21.4	12.1	83.3	<0.1	0.01	0.15	0.78	56.1			
<0.01	71.6	26.2	445	33.9	1.04	11.6	157	<0.1	<0.01	0.08	0.56	11.7			
0.09	8.99	4.89	107	11.5	7.80	7.57	18.6	<0.1	<0.01	0.05	0.20	36.9			

(continued on next page)

Table 1 (*continued*)

ID	Site	Type	X	Y	Depth	T	TDS	pH	Eh	pCO_2	F^-	Cl^-
156	Prataline	w	261654	4676713	45	14.9	213	7.08	170	0.005	0.47	9.94
157	Le Pantane	w	260610	4678097	80	13.4	608	6.80	−20	0.031	0.24	15.7
158	Le Pantane	w	260539	4677952	80	11.6	305	7.21	50	0.006	0.73	27.4
159	Valle Noce	w	262052	4676655	75	14.7	289	7.54	90	0.003	0.16	12.5
160	Castellina	w	263528	4674176	100	9.1	219	7.51	110	0.003	0.06	10.3
161	Ponte Striglia	w	263226	4673765	60	11.4	198	7.27	90	0.003	0.11	14.0
162	Via Lazio	w	263850	4672159	73	13.8	290	7.45	120	0.004	0.10	13.2
163	Acqua Ferrata	s	254392	4659674		12.4	628	4.74	−35	0.360	0.51	74.1
164	Poggio Cinquilla	w	265176	4664051	85	12.9	258	6.98	200	0.008	1.57	15.5
165	Lago Bracciano		266822	4666008		10.9	389	7.99	160	0.002	1.36	40.4
166	La Lega	w	267173	4661132	200	18.4	246	7.09	170	0.008	2.02	12.1
167	Fonticiano	s	266439	4656940		14.9	286	6.82	180	0.010	4.21	17.5
168	Pisciarelli	w	264541	4666386	55	14.7	456	7.30	200	0.011	0.49	8.91
169	Cisterna	s	266003	4665829		15.6	357	6.26	180	0.039	0.72	14.4
170	Ponte Nuovo	s	266245	4667335		10.6	321	7.43	150	0.005	0.36	17.7
171	I Terzi	s	266605	4654775		18.2	305	6.66	140	0.017	1.34	24.7
172	Acqua Acetosa	s	266966	4655380		19.2	1396	5.78	185	0.303	0.91	31.7
173	M. Piantangeli	s	744597	4673430		15.8	233	6.47	150	0.017	0.03	31.7
174	Fonte Cerreta	s	743040	4676603		13.5	284	6.72	210	0.013	0.07	49.8
175	Farnesiana	w	738146	4675943	5	12.7	808	6.86	195	0.042	0.08	42.9
176	Staz. Allumiere	s	737828	4676302		13.8	666	7.27	120	0.012	0.48	57.8
177	Acqua Agra	s	738441	4676550		10.0	2829	6.03	55	0.420	0.38	70.4
178	Fontana Spinare	s	267718	4656863		10.7	302	7.28	200	0.006	1.14	20.1
179	Grotte Civitella	w	269819	4658245	100	20.2	322	7.57	200	0.004	4.80	13.0
180	Vigna di Valle	w	268426	4662015	84	13.2	263	7.50	240	0.002	0.28	18.6
181	Font. dell'Aspro	s	266293	4659497		14.1	335	7.52	212	0.003	0.40	38.8
182	Fonte della Mola	s	261682	4660183		15.4	360	7.86	240	0.002	0.80	15.8
183	Acqua Acetosa	s	261789	4662777		20.1	765	5.48	78	0.178	1.10	17.3
184	Via Trefogliette	w	261122	4664454	55	16.3	510	6.55	40	0.046	0.39	8.87
185	Monte Bischero	s	253312	4657835		15.8	819	7.86	200	0.003	0.58	39.2
186	Bocca Roncone	w	265642	4662483	60	15.0	200	7.50	190	0.002	1.42	10.2
187	Riserva Baccalà	w	260292	4661372	100	13.9	404	7.22	240	0.010	1.55	23.0
188	C. Giuliano	s	261835	4659964		17.7	414	6.31	66	0.043	5.13	18.7
189	Via Trefogliette	s	261332	4664328		13.5	305	6.20	3	0.028	0.45	14.9
190	Fonte del Riccio	s	259227	4661592		15.2	418	4.74	163	0.080	0.30	23.2
191	Mola Vecchia	p	258604	4669106		20.7	2144	2.38	80	0.200	11.4	16.1
192	Mignone	p	258546	4669261		17.8	8605	1.81	326	0.250	11.2	22.0
193	Compr. S. Lucia	s	734953	4670074		18.1	996	6.56	200	0.090	<0.01	46.4
194	Compr. S. Lucia	w	733495	4669556	60	19.7	1664	6.76	185	0.099	0.34	59.2
195	Compr. S. Lucia	w	733783	4669349	60	18.7	972	6.55	118	0.088	0.26	56.1
196	Monte Mignolo	w	242887	4666500	150	20.4	2259	8.06	215	0.008	3.08	78.3
197	Monte Mignolo	w	261135	4677019	120	18.9	733	7.55	−150	0.010	0.59	35.9
S9[a]	Geothermal well	w				20.0	14598	7.93			8.62	6850
SW	Local sea water					20.8	46362	8.22	59		1.17	25864

region of the Sabatini Mountains (e.g. Di Girolamo, 1978; Peccerillo et al., 1984). The volcanic products overlie a sedimentary sequence that comprises, from bottom to top: 1) the thick Mesozoic carbonate formation that represents the main geothermal reservoir of Central Italy; 2) the Cretaceous–Oligocene Ligurian-type allochthonous flyschoid sediments (Tolfa Flysch) and 3) the Miocene–Quaternary neo-autochthonous clay and sand–clay formations. The pre-volcanic sedimentary units are folded and thrusted, producing NW- and NE-striking extensional faults arranged in horst–graben structures (Buonasorte et al., 1987; Barberi et al., 1994). The structural lows of the Meso-Cenozoic units are filled with up to 2000 m thick Neogene marine to continental sand and clay deposits. The anti-Apenninic (roughly E–W oriented) fault system, activated during the Pleistocene, played an important role in controlling the structural and volcanic evolution. Where the acid dome complexes were emplaced, the pre-volcanic basement was uplifted because of the intrusion of these sub-volcanic bodies (Cimarelli and De Rita, 2006).

A large thermal anomaly characterizes the peri-Tyrrhenian sector of Central Italy, with heat flow values locally higher than 200 mW/m^2 (Cataldi et al., 1995), likely associated with volcanic complexes and structural highs of the Mesozoic carbonates (Baldi et al., 1973; Ceccarelli et al., 1987; Minissale and Duchi, 1988).

The main hydrogeological patterns are related to: 1) a regional aquifer hosted in the thick sequence of Mesozoic limestones, and 2) shallow aquifer(s) hosted in the volcanic and sedimentary Plio-Quaternary deposits which locally may show a relatively high permeability (e.g. Dall'Aglio et al., 1994).

3. Methods

Waters and gases (197 and 15 samples, respectively) from cold and thermal springs, wells and bubbling pools were collected from May 2007 to April 2008 within an area of about 700 km^2 extending westward from the western edge of the Bracciano Lake to the Tyrrhenian Sea, near Civitavecchia (Fig. 1).

3.1. Chemical and isotopic ($\delta^{18}O$ and δD) analysis of water samples

Temperature, pH, Eh, electrical conductivity values, and alkalinity (titration with 0.05 N HCl), silica (spectrophotometry) and NH_4 (potentiometry with ion-selective electrode) concentrations were determined in situ. Water samples were filtered (0.45 μm) and stored in high-density polyethylene flacons for laboratory analysis. Major anions (F^-, Cl^-, Br^-, SO_4^{2-} and NO_3^-) and cations (Ca, Mg, Na and K) were analyzed by ion-chromatography (Dionex, DX500) on filtered and filtered and acidified samples, respectively. Minor and trace elements (B, Li and Sr) were determined on filtered and acidified samples by ICP-MS. An unfiltered diluted sample (1:10) was collected for the determination of SiO_2 by molecular spectrophotometry. The analytical error for major and minor and trace compounds error was <5 and 10%, respectively.

Br^-	NO_3^-	SO_4^{2-}	HCO_3^-	Na	K	Mg	Ca	NH_4	Li	B	Sr	SiO_2	$\delta^{18}O$	δD	Elev.
<0.01	15.0	8.26	88.5	17.2	21.0	2.39	12.6	<0.1	0.03	0.13	0.18	75.4			
<0.01	97.0	1.72	329	38.8	26.4	13.4	75.1	<0.1	<0.01	0.05	0.17	19.3			
<0.01	17.9	22.3	134	32.5	24.4	4.28	30.7	<0.1	<0.01	0.02	0.03	21.2			
<0.01	37.7	4.82	134	19.1	11.6	5.68	31.2	<0.1	<0.01	0.06	0.22	62.7			
<0.01	18.7	5.98	107	11.6	8.40	8.42	23.3	<0.1	<0.01	0.03	0.06	51.6			
<0.01	47.0	1.58	67.1	12.4	8.43	7.18	17.0	<0.1	<0.01	0.03	0.19	46.5			
<0.01	27.1	6.95	146	16.7	10.1	12.0	29.5	<0.1	<0.01	0.03	0.45	54.0			
<0.01	4.21	350	0	44.9	3.92	23.9	108	0.50	<0.01	0.09	0.29	17.9	−6.2	−35	230
<0.01	11.3	7.96	116	17.7	32.5	5.43	15.6	<0.1	<0.01	0.07	0.19	67.9			
<0.01	1.58	20.1	201	50.8	42.3	11.0	17.7	<0.1	0.03	0.48	0.68	1.60	0.8	−1	165
0.04	13.3	3.74	122	18.3	23.6	6.80	14.2	<0.1	0.01	0.06	0.20	59.4			
0.08	44.1	10.7	104	33.4	13.2	8.89	15.8	<0.1	<0.01	0.07	0.13	68.7			
<0.01	26.5	5.27	275	15.7	14.9	10.1	64.9	<0.1	<0.01	0.05	0.45	68.4			
<0.01	22.0	10.0	186	21.0	25.9	11.7	27.8	<0.1	<0.01	0.06	0.31	73.7			
0.03	16.9	5.13	171	19.3	19.9	11.3	27.4	<0.1	<0.01	0.05	0.36	62.9			
0.06	23.1	9.67	128	34.1	26.0	7.49	13.8	<0.1	0.02	0.06	0.24	72.9			
<0.01	7.08	3.50	939	102	81.8	40.1	135	1.70	0.11	0.38	1.16	104	−5.8	−35	105
0.04	3.05	11.0	101	29.8	2.72	8.57	16.5	<0.1	0.02	0.06	0.12	56.5			
0.08	1.63	14.6	116	39.1	2.79	11.1	22.2	<0.1	0.04	0.05	0.18	52.3			
<0.01	22.7	22.7	500	37.8	1.67	6.24	168	<0.1	0.01	0.11	0.51	10.6			
<0.01	55.9	54.6	308	56.4	1.59	10.3	115	<0.1	0.02	0.11	0.61	9.42			
0.14	8.02	36.4	1983	68.9	19.4	48.5	581	0.90	0.19	0.22	2.85	15.0	−6.4	−37	105
0.02	17.2	7.22	146	22.4	23.2	9.61	21.0	<0.1	<0.01	0.05	0.26	67.0			
<0.01	7.73	4.04	168	29.7	44.3	5.42	12.1	<0.1	0.03	0.11	0.13	65.0			
0.05	41.5	17.8	94.6	18.6	10.9	11.4	24.4	<0.1	<0.01	0.03	0.32	48.3			
0.12	18.5	19.6	137	30.8	24.4	11.0	24.0	<0.1	<0.01	0.07	0.33	59.2			
<0.01	42.2	13.2	174	28.2	13.8	11.9	32.4	<0.1	<0.01	0.07	0.18	55.1			
<0.01	2.45	10.5	479	48.6	42.1	24.2	64.1	<0.1	0.07	0.18	1.02	108	−6.4	−35	235
<0.01	1.47	38.3	308	13.7	10.3	15.5	75.2	<0.1	<0.01	0.02	0.15	75.5			
0.22	61.2	187	293	39.6	2.44	12.2	164	<0.1	0.01	0.06	1.16	35.9	−5.0	−30	100
<0.01	20.2	5.17	94.6	12.9	11.1	7.71	16.9	<0.1	<0.01	0.02	0.18	38.7			
<0.01	4.46	22.8	220	27.2	24.9	10.9	40.7	<0.1	0.01	0.03	0.29	56.5			
<0.01	2.47	23.4	207	39.5	36.1	6.90	27.9	<0.1	0.04	0.10	0.44	87.7			
<0.01	5.17	42.8	134	18.1	9.04	13.8	32.2	<0.1	<0.01	0.01	0.41	42.5			
<0.01	12.6	19.1	223	29.7	18.5	15.6	41.3	<0.1	0.02	0.06	0.69	68.5			
<0.01	522	1242	0	19.2	16.1	20.3	73.5	<0.1	0.11	0.32	1.34	141	−5.4	−27	188
<0.01	98.2	6949	0	31.0	64.0	68.5	170	<0.1	0.20	0.39	4.16	269	−3.6	−20	180
<0.01	77.6	8.08	616	32.6	4.63	16.5	187	<0.1	<0.01	0.05	0.67	10.8			
<0.01	34.0	198	915	204	4.80	31.5	205	<0.1	0.03	0.17	1.24	14.9	−6.1	−36	124
<0.01	21.7	50.1	586	54.4	4.70	28.9	163	<0.1	0.02	0.11	1.22	10.5			
<0.01	36.1	322	1135	644	10.1	3.63	19.2	<0.1	0.07	1.78	0.17	10.9			
<0.01	32.2	36.1	439	97.8	5.29	31.0	45.3	<0.1	0.04	0.31	0.93	12.1			
0.56		393	1577	5020	430	4.10	47.5	157	12.0			196			
99.5	27.7	3513	186	14009	600	1569	468	<0.1	0.25	15.7	7.71	1.24	1.2	7	

The $^{18}O/^{16}O$ and $^{2}H/^{1}H$ isotopic ratios (expressed as $\delta^{18}O$ and δD ‰ vs. VSMOW) were determined using an Analytical Precision AP 2003 spectrometer and a Finnigan MAT Delta plus spectrometer, respectively. The analytical precision is 0.1‰ for $\delta^{18}O$ and 1‰ for δD. The carbon isotopic ratios of TDIC (Total Dissolved Inorganic Carbon) (expressed as $\delta^{13}C$ ‰ vs. VPDB) were analyzed by mass spectrometry (Finnigan Delta Plus) following the procedure described by Favara et al. (2002).

3.2. Sampling and chemical analysis of gas samples

Free gas samples from bubbling pools were collected using a plastic funnel positioned above the gas emergence. Three aliquots of the gas phase were collected by connecting different gas vials, as follows: 1) two-way 150 mL glass tubes for the determination of the $\delta^{13}C–CO_2$ values; 2) pre-evacuated 150 mL one-way glass tubes filled with 50 mL of a 4 N NaOH solution for the determination of the $\delta^{13}C–CH_4$, δD–CH_4, $^{40}Ar/^{36}Ar$, $^{3}He/^{4}He$ and $^{4}He/^{20}Ne$ values; and 3) pre-evacuated 60 mL one-way glass tubes filled with 20 mL of a 5 N NaOH and 0.15 M Cd $(OH)_2$ suspension for the determination of the chemical composition and the $\delta^{34}S–H_2S$ values. During sampling in the second and third aliquots, water vapor and CO_2 dissolve in the alkaline solution. H_2S is dissolved in the second aliquot, whereas in third aliquot the insoluble salt CdS is formed as H_2S reacts with $Cd(OH)_2$. Low-solubility gas species (N_2, O_2, CO, H_2, He, Ar, Ne, CH_4 and light hydrocarbons) were concentrated in the tube head-space (Giggenbach and Gougel, 1989; Montegrossi et al., 2001; Vaselli et al., 2006). Residual inorganic gases and CH_4 were analyzed by using a Shimadzu 15A gas chromatographic system equipped with a 9 m long molecular sieve column and thermal conductivity detector (TCD). Light hydrocarbons were determined by a Shimadzu 14A gas-chromatograph equipped with a 10 m long stainless steel column ($\phi = 2$ mm) packed with Chromosorb PAW 80/100 mesh coated with 23% SP 1700 and a flame ionization detector (FID). The solid precipitate, separated from the alkaline solution by centrifugation at 4000 rpm for 30 min, was oxidized by H_2O_2 to determine H_2S as SO_4^{2-} by ion-chromatography (Methrom 761) and $\delta^{34}S–H_2S$ values (see below). The alkaline solution was used for determining the CO_2 concentrations as CO_3^{2-} by acidimetric titration with 0.1 N HCl. The analytical error is <5% for the main gas components and <10% for minor and trace gas compounds.

The chemistry of dissolved gases, extracted from 185 water samples collected in glass flasks and sealed by gas tight rubber/teflon plugs according to the method of Capasso and Inguaggiato (1998), was determined by using a Perkin Elmer AutoSystem XL gas chromatograph equipped with FID and TCD, with N_2 and Ar as carrier gases, respectively. Dissolved gas composition (expressed in mmol/L at STP) was calculated from the composition of the exsolved gas phase on the basis of the solubility coefficients of each gas compound (Whitfield, 1978). Analytical error was <5%. The pCO_2 values were computed by using the PHREEQC code v. 2.12 (Parkhurst and Appelo, 1999), operating with the Lawrence Livermore National Laboratory (LLNL) database.

3.3. Isotopic analysis of C ($^{13}C/^{12}C$ ratio of CO_2 and CH_4), H ($^{2}H/^{1}H$ ratio of CH_4), S ($^{34}S/^{32}S$ of H_2S) and He ($^{3}He/^{4}He$ ratio)

The $\delta^{13}C$–CO_2 values were determined by mass spectrometry (Finningan Delta S), after a two-step extraction and purification procedures of the gas mixtures by using liquid N_2 and a solid–liquid mixture of liquid N_2 and trichloroethylene. Internal (Carrara and San Vincenzo marbles) and international (NBS18 and NBS19) standards were used to estimate external precision. The analytical error and the reproducibility are ±0.05‰ and ±0.1‰, respectively.

The values of $\delta^{13}C$–CH_4 and δD–CH_4 were analyzed by mass spectrometry (Varian MAT 250) according to the procedure by Schoell (1980). Analytical precision is ±0.15‰ and ±2.5‰, respectively. The $\delta^{34}S$–H_2S values (expressed as ‰ vs. VCDT) were determined after the precipitation of SO_4^{2-}, deriving from the oxidation of CdS obtained during the gas sampling, as $BaSO_4$ by using a 1 M solution of $BaCl_2$. The $\delta^{34}S$–H_2S analyses were performed with an EA–IRMS system consisting of a 20–20 isotope ratio mass spectrometer (Europa Scientific, Crewe, UK), equipped with an elemental analyser (Sercon Ltd, Crewe, UK). Analytical precision is <0.3‰. Helium isotopic ratios (expressed as R/R_a, where R is the $^{3}He/^{4}He$ measured ratio and R_a is the $^{3}He/^{4}He$ ratio in the air: 1.39×10^{-6}; Mamyrin and Tolstikhin, 1984), as well as the $^{4}He/^{20}Ne$ and $^{40}Ar/^{36}Ar$ ratios, were determined by using a double collector mass spectrometer (VG 5400-TFT) according to method described by Inguaggiato and Rizzo (2004).

4. Results

4.1. Chemical and isotopic composition of waters

Chemical and isotopic ($\delta^{18}O$ and δD) compositions of water samples are reported in Table 1.

Most cold springs have low TDS (<1000 mg/L), slightly acidic to neutral pH, low pCO_2 (from 0.01 to 0.03 bar) and Ca(Mg)–HCO_3 to Na–HCO_3 compositions (Figs. 2a,b). Such chemical features are typical of meteoric waters circulating at relatively shallow depth within volcanic and sedimentary rocks (Dall'Aglio et al., 1994; Chiodini et al., 1995; Frondini, 2008). Some of the cold springs hosted in the volcanic sector, locally known as acque acetose (samples 11, 20, 27, 35, 41, 52, 68, 111, 129, 149, 163, 172, 177, and 183), are characterized by relatively high pCO_2 (up to 0.90 bar), acidic pH (4.7–6.5) and high TDS values (up to 8000 mg/L). A restricted group of cold springs located in the acidic Tolfa Dome Complex area (samples 46, 47, 48, 55, 66, 67, and 75) shows a Na–Cl(SO_4) composition with very low TDS values (100 to 450 mg/L) and pH (3.8 to 5.9).

Thermal springs (>20 °C) have relatively high TDS values (up to 5000 mg/L), temperatures ranging from 21 to 52 °C (Table 1) and Ca–SO_4 composition, except for the Maggiorana well (sample 64) (Fig. 1), which has TDS of 8160 mg/L and a Na–HCO_3 composition (Figs. 3a, b). Thermal waters at Stigliano (samples 38–40) and Borgo Pantani (samples 88–90, 95, 101 and 102) are characterized by relatively high HCO_3^-, Na and Cl^- concentrations (1000–2000, 200–500 and 140–570 mg/L, respectively) and pCO_2 values (up to 0.70 bar).

The chemical features of bubbling pools strongly depend on the chemistry of the associated gas phase (Risacher et al., 2002). Ca(Na)–HCO_3 composition and moderate acidity (pH from 5.2 to 6.6) are related to the presence of CO_2-rich gases (samples 14, 36, 37, 39, 42, 51, 53, 109, 116, 123, 124, 147 and 148), whereas acid–sulfate composition and pH values down to 2 (samples 15, 26, 125, 138, 139, 191 and 192) are associated with an H_2S-rich gas phase.

The $\delta^{18}O$ and δD values, measured in 52 selected samples, range from −41 to −11‰ and from −16.3 to −0.8‰ vs. VSMOW, respectively (Table 1).

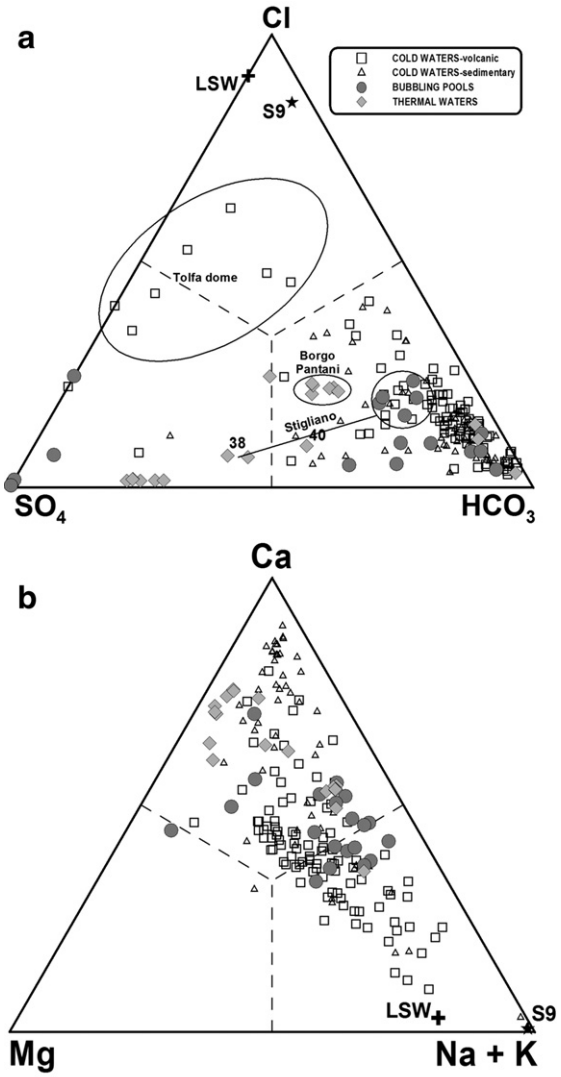

Fig. 2. Ternary diagrams of the main a) anions and b) cations. LSW = local seawater; S9 = geothermal well.

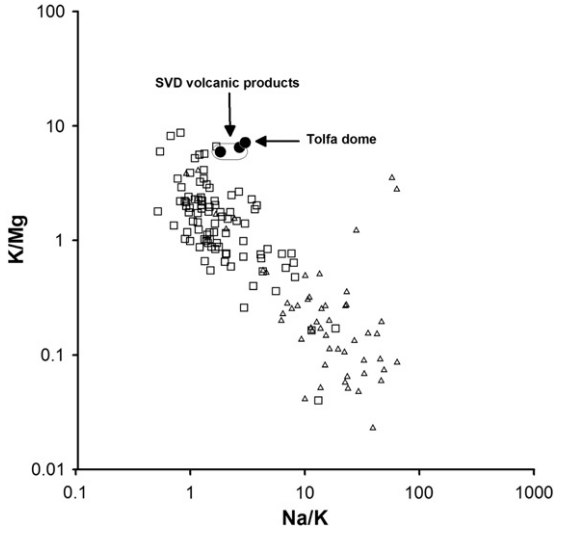

Fig. 3. Na/K vs. K/Mg plot for the cold springs. Note that those emerging from the Quaternary volcanics show ratios similar to those of the host volcanic rocks of the SVD (De Rita et al., 1993). Symbols as in Fig. 2.

4.2. Chemical and isotopic composition of dissolved gases

The main dissolved gas in most cold springs from the shallow volcanic and sedimentary aquifers of SVD and TM is N_2 (up to 1.88 mmol/L). Dominant CO_2 (up to 22.9 mmol/L; Table 2) characterizes the acque acetose (samples 11, 20, 27, 35, 41, 52, 68, 111, 129, 149, 163, 172, 177, and 183) and the thermal springs. The dissolved gases display a relatively wide range of variations in terms of CH_4 (from 5×10^{-7} to 0.09 mmol/L), He (from 3×10^{-6} to 3×10^{-5} mmol/L) and H_2 (7×10^{-9} to 0.002 mmol/L). Oxygen is up to 0.56 mmol/L, whereas CO is below the instrumental detection limit.

The $\delta^{13}C$–TDIC values range from −18.2 to +6.2‰ vs. VPDB (Table 2). The $\delta^{13}C$–CO_2 values (Table 2) were calculated from those of TDIC using the following equation (Zhang et al., 1995):

$$\delta^{13}C_{CO_2(g)} = \delta^{13}C_{TDIC} - \frac{H_2CO_3}{TDIC}\varepsilon_{(H_2CO_3-CO_2)} - \frac{HCO_3^-}{TDIC}\varepsilon_{(HCO_3^- - CO_2)} - \frac{CO_3^{2-}}{TDIC}\varepsilon_{(CO_3^{2-}-CO_2)} \quad (1)$$

which takes into account the equilibrium molar ratios of aqueous carbon species at sampling temperature and pH, computed with the PHREEQC program (Parkhurst and Appelo, 1999), and the isotope enrichment factor (ε) between dissolved carbon species and gaseous CO_2 at the same conditions.

4.3. Chemical and isotopic composition of free gases

The chemical and isotopic (R/Ra, $^4He/^{20}Ne$, $^{40}Ar/^{36}Ar$, $\delta^{34}S$–H_2S, $\delta^{13}C$–CO_2, $\delta^{13}C$–CH_4 and δD–CH_4) compositions of discharging gases are reported in Table 3. Carbon dioxide is by far the most abundant species (>980,589 μmol/mol), with variable concentrations of N_2 (2063 to 16,536 μmol/mol) and CH_4 (98 to 8415 μmol/mol). Hydrogen sulfide is present in considerable amounts (461 to 2178 μmol/mol), with the exception of Poggio del Fattore well (sample 147), where it does not exceed 15.0 μmol/mol. Oxygen concentrations are <420 μmol/mol, indicating low air contribution from shallow depth and/or during the gas sampling. Argon, H_2, He and Ne are present at relatively low concentrations (up to 128, 3.1, 2.4 and 0.07 μmol/mol, respectively). Among light hydrocarbons the most abundant, i.e. C_2H_6 (from 0.069 to 0.357 μmol/mol) and C_3H_8 (from 0.003 to 0.016 μmol/mol), are reported in Table 3. Carbon monoxide is below the detection limit (<1 μmol/mol), possibly because this gas readily dissolves in shallow aquifers forming HCOOH (Shock, 1993). However, time-dependent reactions in the NaOH solution could also explain the lack of CO in the headspace of the sampling flasks (Giggenbach and Matsuo, 1991; Arnórsson et al., 2006).

The $\delta^{13}C$ values in CO_2 ($\delta^{13}C$–CO_2) and CH_4 ($\delta^{13}C$–CH_4) range from −2.8 to +2.7‰ and from −25.7 to −19.5‰ vs. VPDB, respectively, whereas δD–CH_4, range from −152 to −93.4‰ vs. VSMOW. The helium isotopic ratios, corrected for air contamination by using the He/Ne ratio, vary from 0.37 to 0.62 R/R_a, whereas those of argon ($^{40}Ar/^{36}Ar$) are equal to that of air (296). Finally, the $\delta^{34}S$–H_2S values, measured in 6 selected sites, are relatively constant in the SVD area and range from +9.3 to +10.4‰ vs. VCDT (Table 3).

5. Discussion

5.1. Processes governing the chemical and isotopic composition of waters

Low-pCO_2, low-TDS and Ca(Na)–HCO_3 type cold springs are related to shallow aquifer(s) within the SVD and the sedimentary units of the TM. However, the TM springs have relatively higher TDS and pH values than those of the SVD area, likely because leaching during water–rock interaction is more effective on sedimentary rocks (i.e. carbonate-rich rocks) relative to volcanic deposits. Moreover, the SVD springs show relatively high K concentrations with respect to those of TM (Fig. 3), in agreement with the high K content of alkali–potassic rocks of the Roman magmatic province (De Rita et al., 1993).

The distribution of water samples in the HCO_3^- vs. pH binary diagram (Fig. 4), where the saturation curves of CO_2, calculated at pCO_2 values from 0.025 to 0.1 bar, are reported, supports the hypothesis that the chemical features of the acidic cold waters (acque acetose), i.e. high-TDS, high-pCO_2 and a Ca(Na)–HCO_3 composition, depend on significant contribution of CO_2-rich gases favoring gas–water–rock interactions even at low temperatures (i.e., Chiodini et al., 1995; Frondini, 2008). Low-pH (<4) acid-sulfate bubbling pools are produced from the near surface oxidation of H_2S, accompanying CO_2 in the uprising gas phase. The Ca–SO_4 thermal springs have a deep origin related to relatively long circulation paths and water–rock interaction processes with the Triassic anhydrite layers ("Burano" formation) that underlie the Mesozoic limestone formations (Minissale, 2004). Nevertheless, the relatively high HCO_3^- concentrations detected at Stigliano and Borgo Pantani and the Na–HCO_3 composition of Maggiorana well (sample 64) (Fig. 4) likely imply the dissolution of a CO_2-rich gas phase rising from a deep fluid reservoir.

The acidic, low-TDS, Na–Cl(SO_4) springs of the Tolfa Dome area (Fig. 2a) are associated with both shallow waters fed by meteoric waters suffering seawater contamination (marine spray) and interaction with the sulfide-bearing ore deposits of the Tolfa Mountains (Field and Lombardi, 1972; Cavarretta and Tecce, 1987; Cavarretta and Lombardi, 1992).

The δD–$\delta^{18}O$ diagram (Fig. 5a, b) shows that most of the cold and thermal springs plot along the Local Meteoric Water Line (LMWL) inferred by Giggenbach (1988) for precipitations in the Alban Hills area, located about 60 km SE from the study area. On the contrary, most of the bubbling pools are characterized by a strong negative ^{18}O shift, likely produced by isotopic exchange between meteoric water and CO_2, according to the reaction (Negrel et al., 1999):

$$0.5C^{16}O_2 + H_2{}^{18}O \rightarrow 0.5C^{18}O_2 + H_2{}^{16}O \quad (2)$$

The water isotopic composition of the bubbling pools sampled at Sasso (samples 138 and 139) seems to depend on both Reaction (2) and hydrogen isotopic fractionation, the latter being possibly related to H_2S exsolution and/or silicate hydration (Cartwright et al., 2002). Evaporation processes likely control isotopic fractionation of part of the bubbling pools sampled at Manziana and Canale Monterano (samples 15, 191, and 192) (Fig. 5a). Assuming that the recharge area of the local aquifers corresponds to the Tolfa and Sabatini Mountains (Bono et al., 1985; Capelli et al., 2005; Fig. 1), at an altitude of 200–600 m a.s.l. (Fig. 5b), the slight positive $\delta^{18}O$-shift shown by thermal and CO_2-rich cold waters and bubbling pools of Stigliano (samples 36 and 38–42), may be ascribed to isotopic water–rock exchange.

Summarizing, three main interaction processes can be identified to explain the chemical composition of thermal and cold springs in the studied area: 1) weak water–rock interaction involving volcanic and sedimentary formations at relatively shallow depth; 2) dissolution of a CO_2-rich gas phase into the shallow aquifers; and 3) gas–water–rock interactions within a hydrothermal system hosted in Mesozoic carbonates at the top of Triassic anhydrite layers. Shallow waters that are affected by a deep-seated gas input discharge are those of Sasso (samples 138, 139, and 163), Manziana (samples 11, 14, 15, 20, 52, 53, and 183), Canale Monterano (samples 26, 27, 29, 35, 191, and 192), Oriolo (samples 116 and 129), Vejano (samples 109, 111, and 123–125) and Blera (samples 147–149) (Fig. 1). Thermal waters hosted in the Mesozoic limestone formations emerge as springs and bubbling pools at Stigliano (samples 36–42, 51) and Bagnarello (sample 44), while they were sampled from wells at Sasso (samples 106 and 143), Manziana (sample 43), Civitavecchia (samples 76 and

Table 2
Chemical and isotopic composition of dissolved gases, He, H_2, O_2, N_2, CH_4, and CO_2 in mmol/L; $\delta^{13}C$ as ‰ vs. VPDB.

ID	Site	He	H_2	O_2	N_2	CH_4	CO_2	$\delta^{13}C(TDIC)$	$\delta^{13}C(CO_2)$	$R/Ra_{(c)}$	$^4He/^{20}Ne$	^3He	$CO_2/^3He$
1	Precilia	8.6E-06	1.0E-06	0.56	1.70	6.60E-06	0.22	−18.2	−23.1				
2	Villa palombaro	8.3E-06	8.1E-07	0.56	1.68	1.09E-05	0.03						
3	Via Oriolese	5.0E-06	1.6E-06	0.26	1.04	1.12E-04	0.68						
6	Altare rupestre	8.6E-06	1.1E-06	0.57	1.71	9.89E-06	0.06						
7	Quadroni	7.8E-06	5.1E-07	0.49	1.62	5.39E-06	0.41						
8	Vivaio Motosi	3.6E-06	3.6E-07	0.14	0.95	5.96E-05	3.92	−7.8	−10.1				
9	Ponte Mariano	8.2E-06	3.1E-06	0.52	1.69	1.06E-05	0.33						
10	Ponte Mariano												
11	Casa dei Nonni	3.1E-06	3.3E-07	0.13	0.64	4.91E-04	18.4	−3.5	−3.9				
12	Le Grazie	7.4E-06	1.5E-06	0.20	0.82	1.57E-04	8.58						
13	Comune Manziana	3.7E-06	5.8E-08	0.19	0.90	1.48E-05	4.40						
14	Caldara Manziana	3.3E-06	6.4E-07	0.13	0.57	1.75E-04	16.4	−1.8	−2.6				
15	Caldara Manziana	4.3E-06	3.8E-05	0.14	0.68	1.24E-04	10.9	−3.8	−3.0				
16	Fontanile Caldara	4.2E-06	7.5E-07	0.34	1.08	1.82E-05	0.56						
17	Agriturismo Caldara	9.2E-06	9.8E-07	0.57	1.82	5.85E-06	0.08						
18	Ferriere	4.7E-06	5.7E-07	0.20	1.09	9.45E-06	1.07						
19	SP Aurelia-Braccianese	7.5E-06	6.7E-07	0.39	1.28	1.68E-05	0.33						
20	Fosso Lenta	4.6E-06	3.3E-06	0.19	0.71	6.49E-05	20.8	−3.7	−4.1				
22	Comune Canale M.	6.3E-06	5.7E-07	0.45	1.57	3.96E-06	0.49						
23	Lavatoio	5.8E-06	8.0E-07	0.28	1.17	6.80E-04	0.43						
24	Castel Donato	8.6E-06	1.6E-06	0.54	1.65	3.04E-05	0.32						
25	Casa Merenda	1.2E-05	5.4E-06	0.38	1.88	4.86E-06	0.34						
26	Parco di Diosilla	8.2E-06	5.5E-06	0.48	1.53	1.26E-03	5.86	−3.3	−2.5				
27	Fonte Rafanello	8.8E-06	1.4E-06	0.49	1.68	2.38E-04	8.97	−1.1	−3.6				
28	Fonte della Bandita	5.2E-06	1.1E-06	0.34	0.99	6.75E-06	0.28						
29	Fonte del Castagno	3.7E-06	7.6E-07	0.20	0.70	2.75E-06	12.7	−3.5	−3.6				
30	Comune Bracciano	5.2E-06	1.2E-06	0.33	0.93	4.67E-06	0.85						
31	Sorgente Minciaro												
32	Ponton della Mola												
33	Prati di Canale	4.3E-06	6.5E-07	0.21	0.98	2.22E-06	1.63						
34	Quarto Grande	6.0E-06	7.5E-07	0.29	1.24	9.51E-06	0.83						
35	Acqua di Tito	8.9E-06	5.9E-05	0.52	1.67	1.13E-04	1.68	−3.7	−5.8				
36	Piana di Stigliano	6.1E-06	3.0E-06	0.14	0.54	5.94E-04	15.3	2.7	−0.8				
37	Piana di Stigliano	1.1E-05	2.2E-05	0.54	1.72	8.53E-05	3.27	3.1	−1.8				
38	Terme Stigliano	2.7E-05	3.4E-06	0.28	1.19	6.85E-06	2.80	4.0	1.1				
39	Terme Stigliano	1.4E-05	4.8E-06	0.78	2.58	1.74E-05	1.19	3.8	0.5				
40	Terme Stigliano	3.5E-06	3.3E-06	0.13	0.56	2.34E-05	10.3	4.1	1.1				
41	Fontana Rota	6.4E-06	1.0E-06	0.24	1.02	3.10E-06	17.4	5.9	1.2				
42	Rota	4.3E-06	2.8E-06	0.13	0.53	2.83E-03	15.0	6.8	2.2				
43	Casale Acquadoro	1.1E-05	6.0E-05	0.31	1.23	5.91E-04	4.70	1.7	−0.6	0.47	0.13	7.5E-12	6.3E + 11
44	Bagnarello	7.9E-06	3.7E-06	0.20	0.86	2.36E-04	5.57	3.6	1.6				
46	Fonte Limoiola	3.0E-06	5.9E-07	0.13	0.77	2.90E-06	0.82						
47	Fonte Canale	8.0E-06	1.7E-06	0.34	1.34	4.29E-06	0.91						
48	Fonte Lizera	4.7E-06	2.1E-06	0.35	0.97	1.57E-05	0.91						
49	Sorgente della Nocchia	4.6E-06	1.9E-06	0.27	0.87	4.03E-06	0.78						
50	SP Tolfa-S.Severa	5.0E-06	3.3E-06	0.36	1.00	1.12E-05	0.98	−12.9	−20.7				
51	Polla Rota	3.7E-06	1.3E-06	0.12	0.48	5.18E-03	19.7	−1.8	−4.9				
52	Caldara Manziana	1.4E-05	1.3E-06	0.43	1.59	6.29E-06	13.6	6.2	2.0				
53	Via delle Fontanelle	6.5E-06	3.6E-06	0.14	0.65	1.04E-04	11.0	1.3	0.2				
54	Via delle Fontanelle	7.0E-06	1.9E-06	0.33	1.30	1.25E-05	0.48						
55	Comune Tolfa	4.6E-06	3.6E-06	0.16	1.13	2.42E-05	1.43	−18.2	−17.6				
56	Concia	7.3E-06	4.7E-06	0.36	1.40	7.74E-05	1.29						
57	Fonte del Cerrobuco	7.3E-06	2.8E-06	0.39	1.43	3.45E-05	0.32						
58	Fonte le Pantanelle	8.1E-06	2.5E-06	0.48	1.48	8.50E-06	0.30						
59	Fonte M. Castagno	5.8E-06	2.7E-06	0.29	1.17	7.76E-06	0.35						
60	Cesi della Vaccareccia	5.1E-06	2.4E-05	0.20	1.05	1.80E-05	1.59						
61	Sorgente del Giglio	4.2E-06	7.5E-07	0.19	0.91	9.71E-05	1.01	−16.5	−22.6				
62	Sorgente Fontanaccio	4.3E-06	3.6E-06	0.15	0.91	3.19E-05	0.41						
63	Pontonaccio	3.9E-06	5.1E-07	0.25	0.88	9.55E-05	0.87						
64	Maggiorana	7.6E-06	1.2E-06	0.11	0.49	9.10E-02	22.9	3.8	−0.9				
65	Poggio della Stella	4.4E-06	7.2E-06	0.14	0.98	3.05E-04	1.95	−10.2	−16.6				
66	Fonte la Bianca	5.0E-06	1.2E-06	0.19	1.04	5.20E-04	0.81						
67	Fonte del Connuto	4.2E-06	8.1E-07	0.32	0.88	1.25E-05	0.66						
68	Acqua Acetosa	3.4E-06	1.1E-06	0.11	0.49	2.09E-05	20.4	4.1	−1.7				
69	Poggio Selcioso	3.6E-06	6.9E-07	0.15	0.69	1.64E-05	1.73	−6.2	−12.9				
70	Fonte Granciare	5.0E-06	1.1E-06	0.31	0.92	8.24E-06	1.10						
71	Colle di Mezzo	9.8E-06	1.5E-06	0.37	1.18	1.49E-05	0.60						
72	Fonte Porcareccia	5.4E-06	1.6E-06	0.46	0.93	4.22E-05	1.40						
73	Fonte Lappoleta												
74	Poggio Pinese	3.0E-05	1.8E-06	0.26	1.10	2.07E-05	1.02						
75	Campaccio	3.9E-06	1.2E-06	0.15	0.86	3.38E-04	1.78						
76	Terme Ficoncella	6.5E-06	1.5E-05	0.30	1.13	9.22E-05	1.52	0.1	−3.6				
77	Fonte dell'Olmo	4.7E-06	3.2E-07	0.20	0.94	1.37E-05	0.35						
78	Fonte delle Cannucce	5.1E-06	2.1E-06	0.29	0.90	8.93E-06	0.36						
79	Fonte valle Giuncosa	5.2E-06	1.4E-06	0.26	0.97	9.94E-06	0.44						

Table 2 (*continued*)

ID	Site	He	H_2	O_2	N_2	CH_4	CO_2	$\delta^{13}C(TDIC)$	$\delta^{13}C(CO_2)$	$R/Ra_{(c)}$	$^4He/^{20}Ne$	^3He	$CO_2/^3He$
80	Fonte Capannone												
81	Fontana Guarente	4.6E-06	1.0E-06	0.32	0.90	7.85E-06	0.09						
82	Pian Cisterna	4.0E-06	9.9E-07	0.14	0.87	8.39E-06	0.79						
83	Pisciarello di S. Biagio	5.1E-06	1.2E-06	0.33	1.05	5.42E-06	0.35						
84	Poggio Casalavio	5.0E-06	1.2E-06	0.13	0.83	4.80E-05	1.83						
85	Civitavecchia 1	6.5E-06	4.0E-06	0.15	0.73	1.32E-03	7.90	−2.1	−4.3	0.46	0.08	4.2E-12	1.9E+12
86	Fontanile Miniera	4.9E-06	1.1E-06	0.35	0.93	3.83E-06	0.70						
87	Fonte le Catenare	6.6E-06	1.1E-06	0.34	1.10	5.26E-06	1.02						
88	Albani & Ruggeri 1	1.0E-05	1.6E-06	0.17	0.64	2.42E-03	12.9						
89	Albani & Ruggeri 2	4.6E-06	2.7E-06	0.15	0.52	3.09E-03	13.8						
90	Albani & Ruggeri 3	3.7E-06	1.0E-05	0.16	0.56	1.97E-03	12.1	1.9	−0.9	0.60	0.05	3.1E-12	3.9E+12
92	La Frasca	5.8E-06	4.9E-07	0.27	1.12	9.34E-06	0.72						
93	La Frasca	4.4E-06	3.2E-06	0.14	0.88	1.78E-02	3.32	−4.0	−9.3				
94	La Frasca	4.7E-06	1.2E-06	0.14	0.90	2.41E-02	5.22						
95	La Frasca	4.2E-06	2.2E-07	0.15	0.77	3.52E-05	6.86						
96	Campacceto	5.4E-06	7.5E-07	0.34	1.07	1.29E-05	0.46						
97	Monte Rovello	3.6E-06	6.8E-07	0.13	0.53	3.05E-05	19.0	2.7	0.0	0.24	0.11	1.2E-12	1.6E+13
98	Pian dell'Organo	5.1E-06	8.5E-07	0.15	1.03	2.50E-03	0.73						
99	Campo di Marte	5.0E-06	1.4E-07	0.22	1.04	1.11E-05	0.63						
100	Civitavecchia	7.6E-06	8.4E-07	0.35	1.51	6.09E-06	0.48						
101	Albani & Ruggeri 4	3.7E-06	2.4E-06	0.14	0.52	6.17E-03	16.1						
102	Albani & Ruggeri 5	6.4E-06	1.8E-06	0.28	0.99	6.46E-03	12.9						
103	Fonte Pocopane	6.7E-06	4.2E-07	0.37	1.25	6.34E-06	0.48						
104	Tramontana	4.9E-06	1.4E-06	0.22	0.93	1.42E-04	1.48						
105	Casale dei Frati	9.7E-06	1.5E-06	0.40	1.50	7.07E-06	0.83						
106	Dolomiti del Lazio	2.1E-05	8.2E-06	0.29	1.24	7.98E-04	5.84	−2.7	−5.0				
107	Albani & Ruggeri 6	7.3E-06	1.2E-06	0.34	1.46	1.19E-04	1.62						
108	Pian Cisterna	6.8E-06	1.6E-06	0.18	1.18	9.63E-05	0.19						
109	Caldara Vejano	4.0E-06	5.1E-06	0.17	0.65	7.60E-03	24.3	−0.5	−0.5				
110	Fonte Streppaie												
111	Acqua Forte	5.0E-06	1.3E-06	0.16	0.66	3.75E-03	22.5	−0.6	−0.9				
112	Fontanile Sodi	4.3E-06	9.8E-07	0.25	0.89	1.06E-05	0.35						
113	Fonte Vigna Grande												
114	Fonte Vejano	4.6E-06	1.3E-06	0.29	0.84	4.86E-05	0.71						
115	Fonte Serrale	4.6E-06	3.0E-06	0.27	0.92	1.11E-05	0.27						
116	Parco della Mola	3.0E-06	6.4E-06	0.12	0.46	1.35E-02	16.5	0.9	0.2	0.76	0.21	3.2E-12	5.2E+12
117	Fonte Parco d. Mola	4.5E-06	5.1E-06	0.27	0.85	7.84E-06	1.12						
118	Fonte M. Gennaro	4.1E-06	5.8E-07	0.35	0.87	4.16E-06	0.04						
119	Fonte le Pantane												
120	Fonte M. Casella	4.1E-06	3.4E-06	0.36	0.90	1.29E-05	0.28						
121	Pastinello	4.4E-06	2.8E-07	0.16	1.06	3.62E-05	1.09	−8.5	−16.3				
122	Comune Vejano	4.7E-06	7.7E-07	0.23	0.85	2.26E-04	1.89						
123	Caldara Vejano	3.8E-06	6.1E-07	0.18	0.75	3.27E-03	13.1						
124	Caldara Vejano	3.3E-06	2.4E-06	0.14	0.48	1.90E-03	22.2	0.2	0.5	0.71	0.35	3.3E-12	6.8E+12
125	Caldara Vejano	3.1E-06	7.0E-07	0.14	0.50	1.77E-03	20.0	−1.0	−0.2				
126	Fonte Pascolaro	2.8E-06	4.5E-07	0.19	0.52	9.34E-07	0.27						
127	Fonte Cacapece	4.8E-06	5.1E-05	0.34	0.94	5.82E-06	0.53						
128	Fonte Piscinello	3.2E-06	3.7E-07	0.19	0.54	1.96E-05	0.24						
129	Fonte Parco d. Mola	3.3E-06	1.2E-06	0.12	0.47	1.84E-02	22.7	−0.7	−0.3				
130	Civitella di Cesi	4.6E-06	2.2E-07	0.35	0.94	5.43E-05	0.30						
131	Fonte delle 3 Vasche	5.6E-06	5.9E-07	0.33	1.02	1.00E-05	0.16						
132	Fonte di Cammerata	5.3E-06	9.6E-07	0.34	0.96	9.63E-07	1.16						
133	Fonte Vaccarecce												
134	Fonte Lontaneto	9.8E-06	2.8E-06	0.40	1.12	1.51E-06	0.36						
135	Pontone della Sorca	5.7E-06	8.9E-07	0.23	1.06	2.43E-06	0.56						
136	Casale Vaccherecia	4.8E-06	2.1E-03	0.15	0.92	5.14E-04	1.85	−10.5	−16.9				
137	Valle Campane	6.4E-06	7.7E-07	0.22	1.11	1.61E-05	1.27						
138	M. Solferata	1.3E-05	9.6E-05	0.43	1.49	6.45E-03	17.8			0.30	1.21	5.2E-12	3.4E+12
139	M. Solferata	4.0E-06	1.3E-03	0.14	0.55	1.18E-02	26.0	−2.5	−1.7	0.67	0.38	3.7E-12	7.0E+12
140	Fonte Fumarolo	6.7E-06	9.3E-08	0.32	1.31	5.11E-06	0.55						
141	Fonte Sasso	4.4E-06	5.5E-08	0.34	1.01	4.90E-06	0.32						
142	Villa d'Este	5.6E-06	3.7E-08	0.23	1.17	1.53E-05	1.44						
143	Pian della Carlotta	1.3E-05	1.1E-05	0.39	1.39	5.02E-04	4.34	−2.1	−4.3	0.61	0.10	1.1E-11	3.9E+11
144	Oriolo	4.7E-06	6.9E-09	0.38	1.09	6.37E-06	0.17						
145	Strada Fontanella	5.0E-06	2.1E-08	0.38	1.03	5.01E-07	0.30						
146	Vivaio Montevirginio	4.8E-06	1.4E-08	0.34	0.89	6.08E-06	3.53						
147	Poggio del Fattore	9.7E-06	6.2E-07	0.44	1.56	8.31E-06	17.4			1.04	0.36	1.4E-11	1.2E+12
148	Poggio Saracino	4.1E-06	5.3E-04	0.12	0.46	3.04E-06	24.0	5.2	1.2				
149	Acqua Acetosa	1.2E-05	4.6E-08	0.54	1.88	6.01E-06	4.75	5.3	−1.1				
150	Fonte Murata	8.6E-06	5.7E-08	0.51	1.57	1.03E-05	0.81						
151	Fonte della Vergine	7.3E-06	4.1E-08	0.46	1.49	7.13E-06	0.58						
152	Fonte del Sambuco	8.6E-06	3.3E-08	0.48	1.54	1.15E-05	0.17						
153	Fontana la Casentile	7.8E-06	1.4E-07	0.49	1.49	5.17E-06	0.12						
154	Fontana dei Trocchi	4.0E-06	5.4E-08	0.20	0.93	1.44E-06	1.37						
155	Via Santo Ianni	7.9E-06	6.5E-08	0.47	1.51	1.46E-05	0.06						
156	Prataline	5.3E-06	2.8E-08	0.40	1.31	1.06E-04	0.21						

(*continued on next page*)

Table 2 (*continued*)

ID	Site	He	H_2	O_2	N_2	CH_4	CO_2	$\delta^{13}C(TDIC)$	$\delta^{13}C(CO_2)$	$R/Ra_{(c)}$	$^4He/^{20}Ne$	^3He	$CO_2/^3He$
157	Le Pantane	9.2E-06	7.9E-05	0.27	1.29	9.06E-02	1.39						
158	Le Pantane	6.7E-06	3.2E-08	0.41	1.42	1.24E-05	0.17						
159	Valle Noce	8.6E-06	1.8E-06	0.34	1.17	3.19E-06	0.14						
160	Castellina	7.2E-06	1.9E-08	0.36	1.29	2.70E-06	0.16						
161	Ponte Striglia	5.5E-06	6.1E-08	0.48	1.42	4.70E-06	0.19						
162	Via Lazio	7.0E-06	6.3E-08	0.42	1.56	5.78E-06	0.16						
163	Acqua Ferrata	4.1E-06	2.5E-07	0.20	0.96	2.53E-03	10.3	−4.9	−4.3				
164	Poggio Cinquilla	5.3E-06	3.1E-07	0.36	1.43	6.08E-06	0.19						
165	Lago Bracciano	4.2E-06	1.6E-07	0.35	1.02	9.18E-05	0.09						
166	La Lega	5.0E-06	2.2E-07	0.28	1.02	0.00E+00	0.28						
167	Fontanile Fonticiano	4.3E-06	2.1E-07	0.23	1.11	3.27E-05	0.39						
168	Pisciarelli	4.0E-06	7.7E-08	0.29	1.10	7.08E-06	0.30						
169	Cisterna	3.9E-06	0.0E+00	0.27	1.02	0.00E+00	1.62						
170	Ponte Nuovo	3.6E-06	7.3E-08	0.42	1.11	0.00E+00	0.13						
171	I Terzi	3.8E-06	9.4E-07	0.33	0.93	0.00E+00	0.34						
172	Acqua Acetosa	4.0E-06	3.2E-06	0.26	0.81	6.73E-06	13.2	0.9	−0.3				
173	M. Piantangeli	4.0E-06	9.6E-08	0.28	0.97	5.05E-05	0.47						
174	Fonte Cerreta	4.4E-06	5.0E-07	0.35	1.12	0.00E+00	0.55						
175	Farnesiana	5.0E-06	1.7E-07	0.28	1.29	1.88E-05	1.07						
176	Stazione Allumiere	4.1E-06	1.9E-07	0.37	1.06	0.00E+00	0.26						
177	Acqua Agra	3.9E-06	2.2E-07	0.17	0.77	2.49E-03	16.9	3.4	1.0				
178	Fontana Spinare	4.7E-06	0.0E+00	0.43	1.26	0.00E+00	0.23						
179	Grotte Civitella	4.9E-06	2.7E-07	0.27	1.23	3.45E-06	0.22						
180	Vigna di Valle	8.0E-06	1.9E-06	0.32	1.22	5.54E-06	0.21						
181	Fontana dell'Aspro												
182	Fonte della Mola	8.5E-06	1.4E-06	0.58	1.02	1.34E-05	0.22						
183	Acqua Acetosa	6.2E-06	1.4E-06	0.16	0.69	3.70E-05	16.5	−3.3	−3.5				
184	Via Trefogliette	5.7E-06	8.3E-07	0.21	1.19	1.86E-04	1.63						
185	Monte Bischero	5.8E-06	1.5E-06	0.53	1.13	7.07E-04	0.20						
186	Bocca Roncone	4.2E-06	1.1E-06	0.18	0.88	3.07E-05	0.15						
187	Riserva Baccalà												
188	Cascata C. Giuliano	5.2E-06	1.1E-06	0.17	1.03	1.56E-03	1.51						
189	Via Trefogliette	5.9E-06	2.6E-06	0.26	1.22	2.89E-03	0.67						
190	Fonte del Riccio	6.2E-06	1.9E-06	0.26	1.06	3.55E-05	7.66						
191	Mola Vecchia	1.0E-05	2.9E-06	0.48	1.68	1.18E-03	5.89	−3.3	−2.4				
192	Mignone	9.5E-06	8.6E-04	0.29	0.93	1.89E-03	7.18	−3.0	−2.1				
193	Comprensorio S. Lucia	1.1E-05	2.8E-05	0.52	1.78	3.24E-05	0.59						
194	Comprensorio S. Lucia	1.1E-05	6.1E-06	0.40	1.57	2.56E-05	2.41	−2.9	−8.9				
195	Comprensorio S. Lucia	8.4E-06	2.5E-06	0.45	1.52	1.10E-05	0.79						
196	Monte Mignolo	7.4E-06	2.1E-06	0.29	1.33	4.63E-05	0.45						
197	Monte Mignolo	5.5E-06	6.6E-07	0.26	1.15	9.53E-05	0.51						

85), Tolfa (samples 60, 64, 69, and 97) and Borgo Pantani (samples 88–90, 101, and 102).

In the Sr vs. SO_4^{2-} diagram (Fig. 6), waters related to near-surface oxidation of H_2S (bubbling pools) can clearly be distinguished from those controlled by the interaction with sulfate-bearing evaporitic deposits at depth, since the dissolution of anhydrite is the main Sr source in waters (Barbieri et al., 1979; Minissale et al., 1997b). The only exception is represented by the bubbling pools sampled in the Stigliano area, whose chemical features resemble those of the thermal springs, suggesting a common (deep) sulfate source.

The Na vs. Cl^- binary diagram (Fig. 7a) evidences that the Stigliano and Borgo Pantani waters have relatively high Na and Cl^- concentrations, which may tentatively be ascribed to fluid contribution from 1) a deep geothermal brine or, alternatively, 2) a saline aquifer that is occasionally present in the Neogene marine sediments (Calamai et al., 1976; Duchi et al., 1992; Dall'Aglio et al., 1994; Minissale et al., 1997b). The Stigliano samples are characterized by relatively high B/Cl and NH_4/Cl ratios (Figs. 7b, c) that, coupled with their ^{18}O isotopic shift, seem to support the former hypothesis. On the contrary, the Borgo Pantani waters, having low B/Cl and NH_4/Cl ratios and a meteoric ^{18}O isotopic signature, can be referred to the interaction with fluids trapped in marine clays. The Na/Cl^- ratios of these waters, which are higher than both those of local seawater and the S9 geothermal well (Fig. 7a), are related to Na-enrichment likely caused by intense rock–fluid interaction. This process may also explain the chemistry of the two Na–HCO_3 waters (samples 41, 64). The relatively high Li/Cl^- ratios (Fig. 7d) support this hypothesis, since Li is a conservative element released in natural waters mainly from rock leaching (i.e. Shaw and Sturchio, 1992).

5.2. Origin of gas components

5.2.1. Inert gases (N_2, He, and Ar)

As shown in the N_2–He–Ar ternary diagram (Giggenbach, 1992) (Fig. 8), the SVD-TM gases, with the exception of Poggio del Fattore (sample 147), have N_2/Ar ratios significantly higher (up to 2811) than that of air ($N_2/Ar_{air} = 83$), indicating a non-atmospheric source for N_2, such as 1) gases produced from maturation of organic matter buried in sedimentary formations and 2) those from igneous and metamorphic basement rocks (Jenden et al., 1988; Ballentine and Sherwood Lollar, 2002 and references therein). Nitrogen is fixed as NH_4 in K-rich minerals (micas and K-feldspars) of crystalline rocks and then released as N_2 during metamorphism (Honma and Itihara, 1981) and fluid–rock interaction (Mingram and Brauer, 2001). A metasedimentary N_2 source from the rocks of the Paleozoic basement was suggested for the central Italy gas manifestations on the basis of the $\delta^{15}N$ signature (Minissale et al., 1997a; Minissale et al., 2002). If we consider that argon in SVD-TM gases is totally atmospheric, since the $^{40}Ar/^{36}Ar$ ratio (Table 3) are equal to that of air (296), N_2-excess can be calculated by applying the formula:

$$N_{2(excess)} = \left[\left(\frac{N_2}{Ar}\right)_{meas} - \left(\frac{N_2}{Ar}\right)_{ASW}\right] \times Ar_{meas}. \quad (3)$$

where $(N_2/Ar)_{asw} = 38$ (Fischer et al., 1998). According to Eq. (3), the non-atmospheric N_2 fraction in the SVD gases is from 91 to 99% of total N_2 for most of the SVD-TM gases.

Table 3
Chemical and isotopic composition of the gas discharges. Gas contents are in μmol/mol; $\delta^{13}C$ in CO_2 and CH_4 as ‰ vs. VPDB; δD in CH_4 as ‰ vs. VSMOW; $\delta^{34}S$ as ‰ vs. VCDT; $\delta^{13}C(CH_4)$, $\delta D(CH_4)$, $\delta^{34}S$, R/R_a, $^{40}Ar/^{36}Ar$ and $^4He/^{20}Ne$ ratios are presented for a selected number of samples.

ID	Site	CO_2	H_2S	N_2	CH_4	Ar	CO	O_2	Ne	H_2	He	C_2H_6	C_3H_8	R/Ra	$^4He/^{20}Ne$	$^{40}Ar/^{36}Ar$	$\delta^{13}C(CO_2)$	$\delta^{13}C(CH_4)$	$\delta D(CH_4)$	$\delta^{34}S$	^3He	$CO_2/^3He$	$CH_4/^3He$
15	Caldara Manziana	990641	539	6637	2165	6.0		11	0.003	0.48	1.03	0.113	0.009				−2.79						
15bis	Caldara Manziana	980589	566	16536	2290	5.9	0.05[a]	9.1	0.003	1.36	2.40	0.238	0.016	0.59	1.10	295	−2.18	−25.7	−101	10.4		5.2E+11	1.4E+08
26	Parco di Diosilla	990998	506	5443	3041	3.8		5.0	0.002	0.84	2.17	0.140	0.009	0.57	190	296	−1.83	−22.1	−152	10.2	1.9E-06	1.9E+12	5.8E+09
29	Fonte del Castagno	986773	655	4974	7575	8.0		13	0.005	1.14	0.66	0.357	0.013				−2.53				5.2E-07		
36	Piana di Stigliano	992914	757	2741	3568	6.6		12	0.004	1.13	0.56	0.117	0.003				−0.82						
37	Piana di Stigliano	991557	566	3820	4020	6.2		30	0.004	0.76	0.68	0.158	0.004	0.48	3.95	296	−1.66	−21.2	−116	9.26		1.6E+12	6.6E+09
42	Rota	995004	461	2063	2463	3.3		4.3	0.002	0.40	0.84	0.069	0.013				2.69				6.1E-07		
42bis	Rota	992707	515	3151	3555	21		48	0.012	0.98	0.75	0.078	0.012										
116	Parco della Mola	984952	567	5663	8415	9.8	0.10[a]	388	0.006	3.11	1.29	0.331	0.013	0.62	108	296	0.00	−20.4	−137	9.61		2.1E+12	1.8E+10
123	Caldara Vejano	992094	540	3614	3731	4.1	0.05[a]	15	0.002	1.38	0.55	0.114	0.005	0.59	578	296	0.46	−19.5	−137	10.3	4.7E-07	1.6E+12	6.2E+09
123bis	Caldara Vejano	990717	915	4162	4159	6.5		38	0.004	1.35	0.73	0.163	0.006				0.01				6.0E-07		
139	M. Solferata	985487	2178	6788	5201	10	0.07[a]	332	0.006	1.92	1.26	0.266	0.011	0.37	488	295	−1.14	−23.3	−132	10.1		1.2E+12	6.4E+09
147	Poggio del Fattore	992047	15	7290	98	128		420	0.070	0.05	1.60	0.097	0.005		0.62	296	−0.60	−25.7	−93.4		8.1E-07	1.6E+12	1.6E+08
191	Monte Mignolo	992343	659	4013	2947	7.3		30	0.004	0.47	0.62	0.171	0.005				0.06				6.2E-07		
192	Monte Mignolo	991456	599	4188	3713	5.6		37	0.003	0.89	0.49	0.219	0.006				−0.07						

[a] Data from Minissale (2004).

Fig. 4. HCO_3 vs. pH binary diagram for the collected waters. The CO_2 saturation curves at $pCO_2 = 0.1$, 0.05 and 0.025 bar are also reported. Symbols as in Fig. 2. The rounded rectangle area in is related to the Stigliano and Borgo Pantani samples.

Helium isotopic composition reflects the production of ^4He from radioactive decay processes within the continental crust and the escape of primordial mantle ^3He from zones of active extension or young volcanism. Typical crustal values of R/R_a are in the range 0.01–0.1, while mantle values range between 5 and 8 according to the degree of crustal contamination of the mantle source (Marty and Jambon, 1987; Poreda and Craig, 1989; Hilton et al., 1993; Hulston and Lupton, 1996). The presence of mantle He can be ascertained when $R/R_a > 0.2$ (Mamyrin and Tolstikhin, 1984; Marty et al., 1992). The spatial distribution of mantle ^3He in the peri-Tyrrhenian sector of central and southern Italy was widely investigated in the past (e.g. Hooker et al., 1985; Minissale et al., 1997a; Minissale, 2004). Relatively high R/R_a values (6.9) were measured in gases discharged from active volcanic areas of Etna (Allard et al., 1997), where continental crust is thought to be absent (Marty et al., 1994), and Vulcano (6.0–6.2 R/R_a; Tedesco and Scarsi, 1999). Lower R/R_a values were measured on hydrothermal systems at Campi Flegrei (2.0–3.2 R/R_a; Tedesco et al., 1990), Vesuvius (2.2–2.7 R/R_a; Federico et al., 2002) and Ischia (1.6–3.7 R/R_a; Inguaggiato et al., 2000). In the peri-Tyrrhenian area of Tuscany and Latium (Central Italy) the gases have generally relatively low R/R_a values (from 0.4 to 0.8), although a significant ^3He enrichment was measured in geothermal fluids from Larderello (0.6–3.2 R/R_a; Hooker et al., 1985) and Cesano (1.2–2.0 R/R_a; Minissale et al., 1997a) and in the gas discharges from the Alban Hills (0.9–1.9 R/R_a; Barberi et al., 2007). The R/R_a values of SVD gases (from 0.37 to 0.62) are in the range of those of peri-Tyrrhenian sector of Central Italy. Assuming the R/R_a value of Etna fluids as that typical of the local mantle source beneath Italy (Marty et al., 1994; Magro et al., 2003), the R/R_a values of SVD gases would suggest only a minor mantle contribution and a dominant crustal origin of He. This suggests that the strong N_2-excess measured in the SVD gases is related to contribution of crustal fluids. On the other hand, the general northward decrease of R/R_a values in gas manifestations and fluid inclusions in olivine and clinopyroxene phenocrysts of the Quaternary rocks of central and southern Italy (Martelli et al., 2008) was interpreted as due to the different assimilation by the mantle of crustal material involved in the subduction of the Ionian Adriatic plate (Tedesco et al., 1990; Marty et al., 1994; Peccerillo, 1999).

5.2.2. Carbon species

Two main hypotheses were invoked to explain the origin of deeply derived CO_2 discharging from gas emissions, thermal and cold springs in Central Italy: 1) mantle degassing and 2) thermo-metamorphic

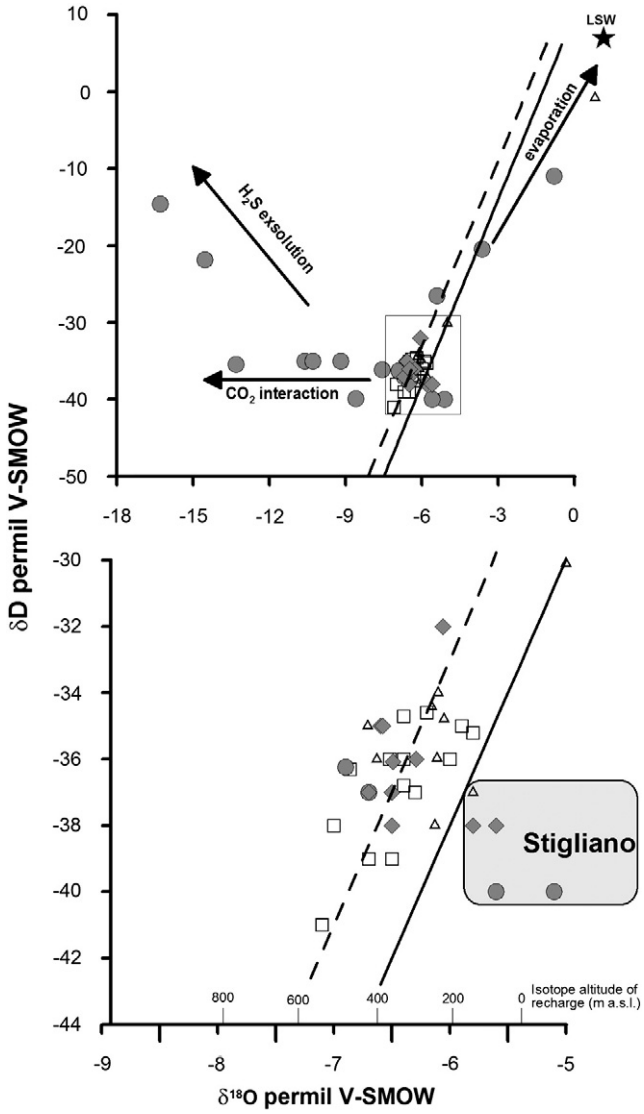

Fig. 5. a) δD–$\delta^{18}O$ scatter plot for the collected waters. The solid and the dashed lines delineate the isotopic domain for Global Meteoric Waters ($\delta D = 8\delta^{18}O + 10$; Craig, 1961) and that for local precipitations ($\delta D = 8\delta^{18}O + 15$; Giggenbach, 1988), respectively. LSW = local seawater; b) detailed scale showing the isotopic shift of the samples of the Stigliano area and the isotopic altitude of recharge. Symbols as in Fig. 2.

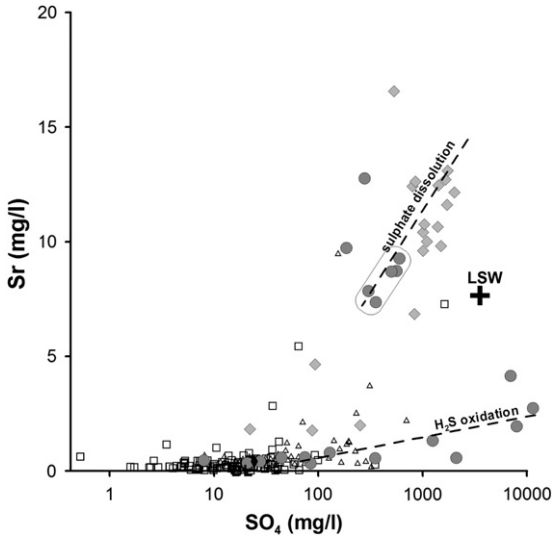

Fig. 6. SO_4^{2-} vs. Sr plot for the collected waters. Symbols as in Fig. 2. Stigliano pools (rounded rectangle area in the plot) are related to interaction with evaporitic sulfates at depth rather than to near-surface oxidation of H_2S.

reactions within the Mesozoic limestone and/or the metamorphic basement of the Tuscan series (e.g. Minissale et al., 1997a; Chiodini et al., 1995, 1999, 2000; Minissale, 2004).

As shown in Fig. 9a, the $\delta^{13}C$–CO_2 values of the sampled waters (−23.0 to +2.3‰ vs. VPDB) suggest that CO_2 is related to different sources: relatively negative $\delta^{13}C$–CO_2 values of the CO_2-poor waters imply dominant CO_2 contribution from plant-root respiration and aerobic decay of organic matter (Cerling et al., 1991); conversely, less negative $\delta^{13}C$–CO_2 values (from −5.8 to +2.3‰ vs. VPDB) in the CO_2-rich waters point to thermo-metamorphic reactions involving carbonate formations ($\delta^{13}C$–CO_2 values from −2.0 to +2.0‰ vs. VPDB; Craig, 1963), although a contribution from mantle degassing ($\delta^{13}C$–CO_2 values from −7.0 to −3.0‰ vs. VPDB; Javoy et al., 1982; Rollinson, 1993) cannot be ruled out.

Relatively high $CO_2/^3He$ ratios (up to 1.6×10^{13}), which are up to four orders of magnitude higher than those of MORB and OIB gases (Des Marais and Moore, 1984; Marty and Jambon, 1987), were measured in bubbling gases and CO_2-rich waters. The $CO_2/^3He$ vs. $\delta^{13}C$–CO_2 diagram (Fig. 9b), where MORB, organic sediment and marine limestone compositions are also reported (Sano and Marty, 1995), confirms that CO_2 in the study area is mainly deriving from thermo-metamorphic decarbonation, with only a minor contribution from the mantle. The prevailing crustal source of CO_2 agrees with the low R/R_a values of SVD gases and CO_2-rich waters.

Methane genetic processes in sedimentary environments are classified as either “biogenic” or “thermogenic”, i.e. related to bacteria-driven or thermal (T > 150 °C) degradation of sedimentary organic matter, respectively, on the basis of its stable carbon and hydrogen isotopic compositions and the relative abundances of co-existing longer-chained hydrocarbons (e.g. Welhan and Craig, 1979; Schoell, 1980, 1988; Rice and Claypool, 1981; Oremland et al., 1987; Welhan et al., 1988; Whiticar and Suess, 1990; Kiyosu et al., 1992; Darling, 1998; Whiticar, 1999; Bréas et al., 2001). Laboratory experiments carried out over the past decades have demonstrated that a variety of low temperature water–rock interactions involving inorganic material are able to efficiently produce both CH_4 and higher hydrocarbons, such as C_2H_6, C_3H_8, and C_4H_{10}, including: 1) reduction of graphite, 2) thermal decomposition of siderite and 3) vapor–water–rock reactions such as serpentinization (Holloway, 1984; Yuen et al., 1990; Berndt et al., 1996; Hu et al., 1998; Horita and Berndt, 1999; McCollom, 2003; Foustoukos and Seyfried, 2004; McCollom and Seewald, 2007). Although the natural occurrence of pure inorganic CH_4 production is still a matter of debate (e.g. Sugisaki and Mimura, 1994; Kenney, 1995; Abrajano et al., 1988; Szatmari, 1989; Giggenbach, 1997; Sherwood Lollar et al., 2002; Taran et al., 2002), recent investigations have reported convincing evidence supporting the presence of CH_4 originated by Fischer–Tropsch Type (FTT) synthesis (Fischer and Tropsch, 1926; Kugler et al., 1979; Anderson, 1984; Bell, 1986; Charlou et al., 1997; Holm and Charlou, 2001), and Sabatier reaction involving CO_2 and H_2 at high temperature and pressure in hydrothermal gases of volcanic environment characterized by high CH_4/C_2H_6 ratios (>250) and $\delta^{13}C$–CH_4 values <−25‰ vs. VPDB (Fiebig et al., 2007; 2009). Isotopic approaches are an effective tool to constrain the origin and mechanism of CH_4 formation in natural systems (e.g. Schoell, 1988; Whiticar, 1999). As shown in Fig. 10, the $\delta^{13}C$–CH_4 and δD–CH_4 values and the composition of the light alkanes of the SVD-TM gases suggest that CH_4 may derive from both abiogenic and thermogenic sources. According to this hypothesis, the $CH_4/^3He$ ratios, ranging between 1.3×10^8 and 8.9×10^9, are intermediate between those measured in sediment-free mid-ocean ridge environment (between 1×10^5 and 1×10^6; Snyder et al., 2003) and those of thermogenic gases (up to 1×10^{12}; Poreda et al., 1988).

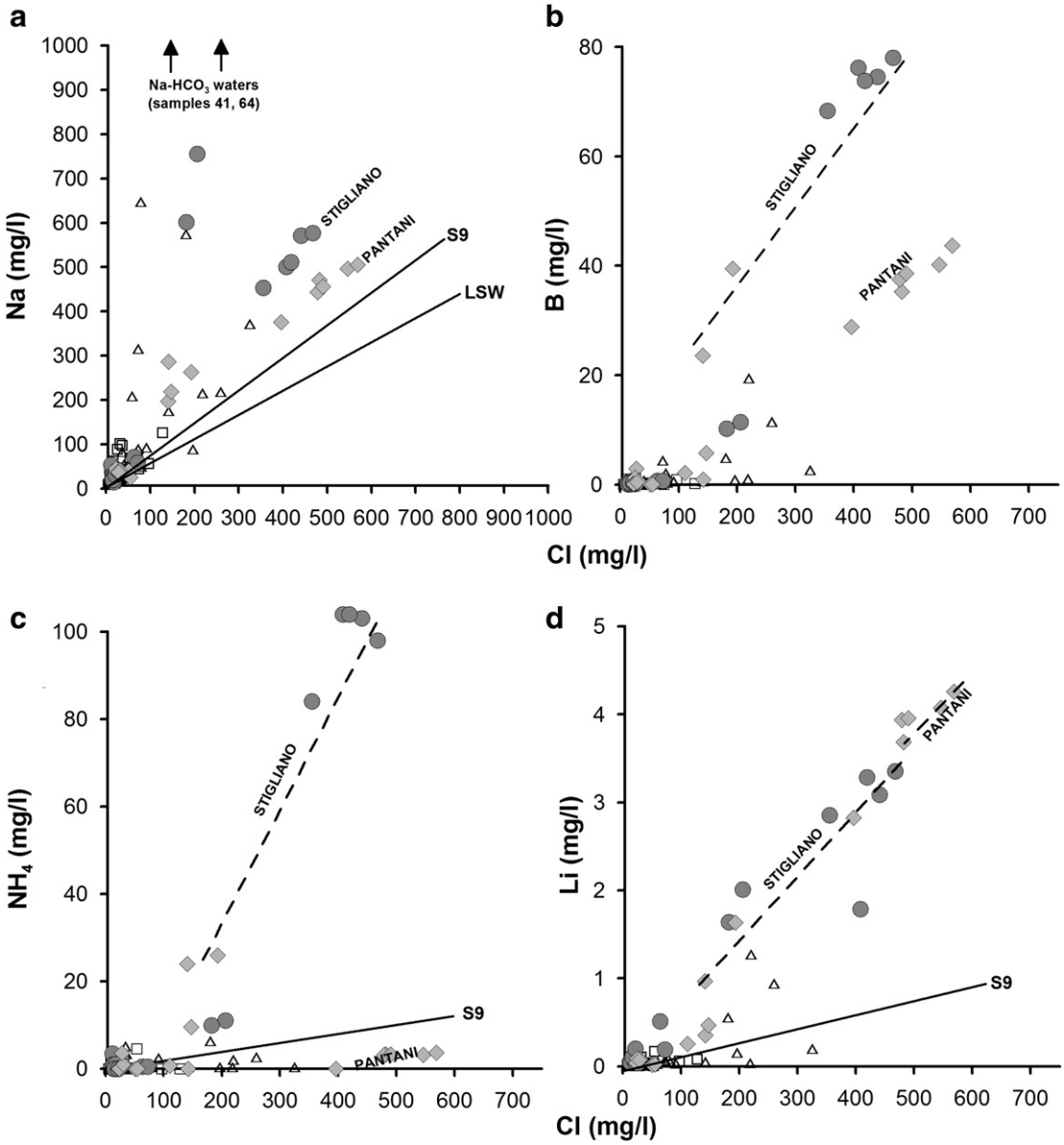

Fig. 7. (a) Na vs. Cl^-, (b) B vs. Cl^-, (c) NH_4 vs. Cl^- and (d) Li vs. Cl^- correlation plots for the collected waters. The dashed lines delineate the trends for Borgo Pantani and Stigliano samples. The solid lines LSW and S9 are representative of the local seawater and the deep geothermal end-member, respectively. Symbols as in Fig. 2.

5.2.3. Hydrogen sulfide

Hydrogen sulfide is by far the most abundant sulfur gas compound in hydrothermal systems (Ohmoto and Lasaga, 1982; Giggenbach, 1980; 1997). Other sources of H_2S in natural gases include magmatic and sedimentary environments. In magmatic systems H_2S is produced by the disproportion of SO_2 during magma degassing and condensation of the vapor plume (Giggenbach, 1987; Allard et al., 1991; Rye et al., 1992; Rowe, 1994). In sedimentary systems the main processes of H_2S generation include: 1) alteration of sulfide minerals (e.g. pyrite; Giggenbach, 1980; Chiodini, 1994), 2) reactions of bacterial and thermochemical sulfate reduction (e.g. Krouse et al., 1988; Kiyosu and Krouse, 1990; Machel et al., 1995; Worden and Smalley, 1996; Marini et al., 2000; Canfield, 2001; Cross et al., 2004; Wynn et al., 2010), and 3) emission from anoxic ocean waters and shallow littoral sediments rich in organic matter (Thode, 1991). Sulfur isotopic composition may provide useful indication to highlight H_2S origin (Ault and Kulp, 1959; Sakai, 1968; Allard et al., 1991; Rowe, 1994; Marini et al., 2000, 2002). Previous investigations focusing on the sulfur isotopic composition of minerals and fluids in Central Italy produced a number of $\delta^{34}S$ data on dissolved SO_4^{2-} and H_2S in springs, native sulfur and on a variety of S-minerals (Field and Lombardi, 1972; Zuppi et al., 1974; Cortecci et al., 1981; Cavarretta and Lombardi, 1992; Grassi and Cortecci, 2005). Conversely, no $\delta^{34}S$–H_2S values are available. $\delta^{34}S$ values for hydrothermal sulfide deposits in the SVD-TM range between −9.5 and +2.7‰ vs. VCDT, whereas the acidic products of the Tolfa Volcanic Dome show values from +1.8 to +13.5‰ (Field and Lombardi, 1972; Cavarretta and Lombardi, 1992). Evaporitic sulfates from Triassic terrains (Burano Formation) show values ranging from +13.6 to +17.4‰ (Cortecci et al., 1981). Dissolved sulfates interpreted as derived from interaction with Triassic anhydrites at depth show $\delta^{34}S$ values generally clustering around +14‰ (Zuppi et al., 1974; Cavarretta and Lombardi, 1992; Grassi and Cortecci, 2005), and aqueous sulfides (S^{2-}) have negative values (averaging −6.8‰). The $\delta^{34}S$–H_2S values of the SVD-TM gases (from +9.3 to +10.4‰ vs. VCDT) seem to exclude an igneous source for H_2S, since the magma-derived sulfur in volcanic rocks and gases

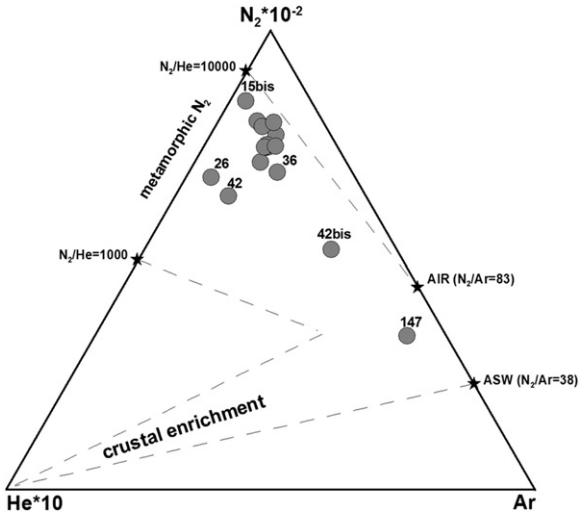

Fig. 8. Ar–N_2–He ternary diagram for free gases. Concentrations are expressed in μmol/mol. ASW = air saturated water at 20 °C.

has $\delta^{34}S$–H_2S ~ 0‰ (Allard et al., 1991 and references therein). A possible sedimentary source of H_2S is related to reduction of sulfates at depth, as follows (Giggenbach, 1980):

$$CaSO_4 + CO_2 + 4H_2 \leftrightarrow CaCO_3 + H_2S + 3H_2O \quad (4)$$

As previously mentioned, the SVD-TM evaporitic Triassic $\delta^{34}S$ values are from +13.6 to +17.4‰ vs. VCDT, i.e. significantly more positive than those characterizing H_2S (Table 3). This implies that H_2S production from Triassic anhydrites has an ε = 3–8‰, which is consistent with theoretical sulfur isotope fractionation at temperatures ≥200 °C (Ohmoto and Rye, 1979; Machel et al., 1995 and references therein).

6. Geothermometry

As shown in the Na–K–$Mg^{1/2}$ triangular diagram of Giggenbach (1988) (Fig. 11), both cold and thermal waters, with the only exception of the Maggiorana well (sample 64) that seems to be partially equilibrated at temperatures of 60–80 °C, are characterized by relatively high Mg concentrations, and thus they can be defined as "immature waters". When the complete equilibrium between fluids and host rocks is not attained, the application of solute geothermometers does not provide realistic estimations of fluid temperatures at depth. Accordingly, the quartz geothermometer (Verma and Santoyo, 1997) provides calculated temperatures <150 °C. This suggests that even along the main tectonic lineaments, where the rising of deep fluids is favored, the chemistry of the water discharges is affected by the presence of shallow aquifers. Conversely, low soluble gas compounds released from the deep fluid reservoir, i.e. CO_2, CH_4 and H_2, are able to reach the surface with no significant compositional changes. Thus, a reliable geothermometric evaluation based on the SVD-TM gas chemistry has to be restricted to gas equilibria in the CO_2–CH_4–H_2 system. Assuming that the CH_4–CO_2 pair is regulated by the Fischer–Tropsch type reaction, as follows:

$$CH_4 + 2H_2O \leftrightarrow CO_2 + 4H_2 \quad (5)$$

the dependence of the $\log(X_{CO2}/X_{CH4})$ values (where X_{CO2} and X_{CH4} are the mole fractions of CO_2 and CH_4, respectively) on temperature in steam produced by boiling of a liquid phase is given by:

$$log\left(\frac{X_{CH_4}}{X_{CO_2}}\right)_V = 4R_H + \frac{5181}{T(K)}, \quad (6)$$

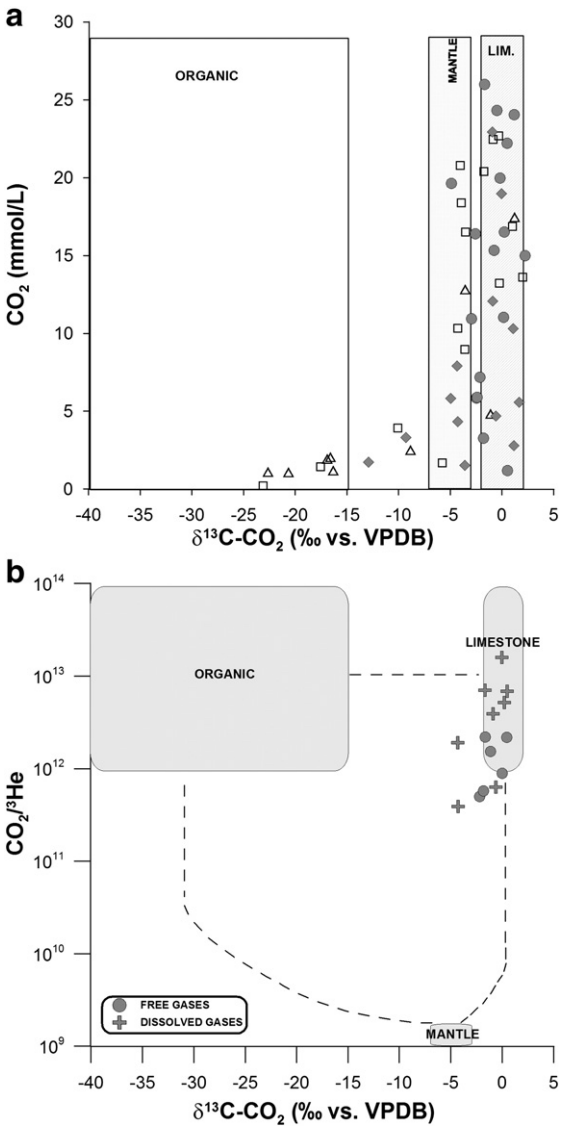

Fig. 9. (a) $\delta^{13}C$–CO_2 in equilibrium with water plotted vs. dissolved CO_2 content (as mmol/L). Symbols as in Fig. 2; (b) $CO_2/^3He$ vs. $\delta^{13}C$–CO_2 correlation plot for free gases and CO_2-rich waters. Boxes and mixing curves between the three end-members are from Sano and Marty (1995).

where $R_H = \log(H_2/H_2O)$ (Giggenbach, 1987). In the liquid phase the $\log(X_{CO2}/X_{CH4})$ values also depend on the vapor/liquid distribution coefficients of CO_2 and CH_4 (B_{CO2} and B_{CH4}, respectively), as follows:

$$log\left(\frac{X_{CH_4}}{X_{CO_2}}\right)_L = 4R_H + \frac{5181}{T} + log\left(B_{CO_2}\right) - log\left(B_{CH_4}\right). \quad (7)$$

Assuming that Ar concentration in hydrothermal fluids is equal to that of air-saturated water (ASW) (Giggenbach, 1991), the dependence of H_2 on R_H in vapor produced by a boiling aquifer is given by:

$$log\left(\frac{X_{H_2}}{X_{Ar}}\right)_V = R_H + 6.52, \quad (8)$$

whereas in the liquid phase is, as follows:

$$log\left(\frac{X_{H_2}}{X_{Ar}}\right)_L = R_H - log\left(B_{H_2}\right) + 6.52, \quad (9)$$

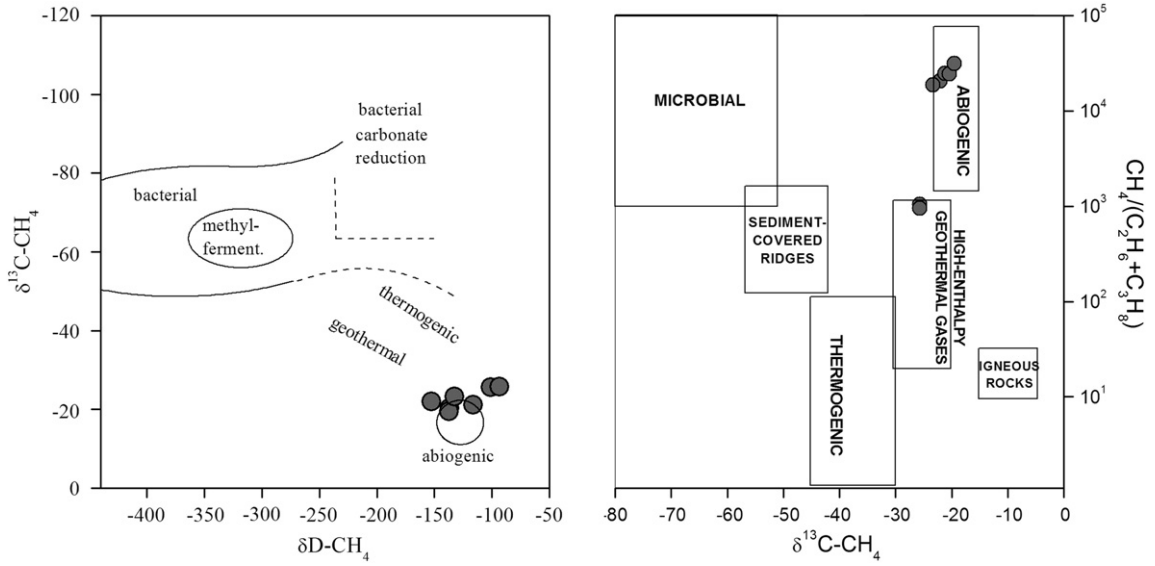

Fig. 10. (a) $\delta^{13}C$–CH_4 vs. δD–CH_4 and (b) $CH_4/(C_2H_6+C_3H_8)$ vs. $\delta^{13}C$–CH_4 diagrams for the SVD gases. Fields and boxes are from Whiticar (1999) and Hunt (1996), respectively.

where B_{H2} is the H_2 vapor/liquid distribution coefficient. The $\log(X_{H2}/X_{Ar^*})$ vs. $\log(X_{CH4}/X_{CO2})$ plot (Fig. 12; Giggenbach, 1993), where the vapor–liquid equilibrium grid at R_H ranging from −3.6 to −2.8 and temperatures from 125 to 374 °C are reported, is constructed according to Eqs. (6), (7), (8) and (9), and adopting B_{CO2}, B_{CH4} and B_{H2} values as reported by Sepulveda et al. (2007). Considering that O_2 is absent in pristine hydrothermal fluids, Ar* values (equal to $Ar–O_2/22$) were used to avoid effects of atmospheric contamination. The CO_2–CH_4–H_2 geothermometer shows that the SVD-TM gases seem to equilibrate in a liquid phase at temperatures ranging between 150 and 200 °C and R_H values between −3.4 and −3.6. This temperature range is significantly lower than those recorded in deep boreholes of the area (up to 290 °C; Cavarretta and Tecce, 1987). However, it has to be considered that H_2 rapidly responds to temperature changes related to the ascent of deep-originated fluids to the surface (e.g. Giggenbach, 1987). This may imply that data points in Fig. 12 plot at lower temperatures than those regulating the CO_2–CH_4 pair at depth due to H_2 re-equilibrium during fluid uprising. Moreover, redox conditions of the CO_2–CH_4–H_2 equilibria are more oxidizing than those ($R_H = -2.8$) typically controlling hydrothermal fluids (Giggenbach, 1987). Such negative R_H values of the SVD gases may be justified considering vapor–liquid interactions at ~200 °C, i.e. temperatures consistent with those calculated by the CO_2–CH_4–H_2 system. This suggests that the CO_2–CH_4–H_2 geothermometer strongly depends on H_2 re-equilibrium at decreasing temperatures. Setting aside Poggio del Fattore well (sample 147), equilibrium temperatures of the CH_4–CO_2 redox pair calculated by Eq. (7) at $R_H = -2.8$ are indeed between 260 and 310 °C, that can be considered reliable for the SVD-TM hydrothermal fluids.

The application of the hydrogen sulfide geothermometer is based on the assumption that the concentration of H_2S in hydrothermal

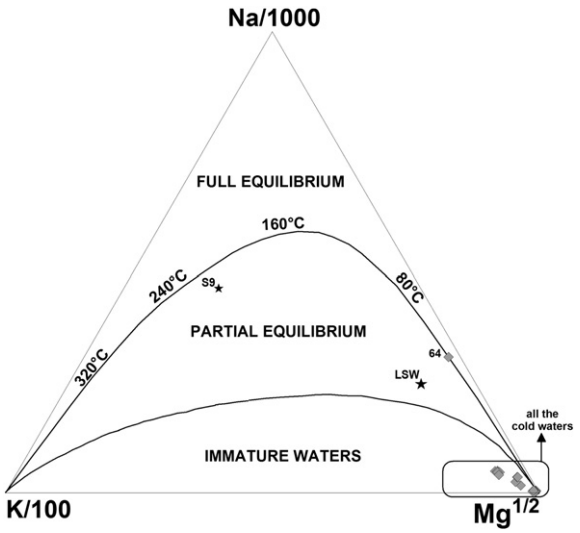

Fig. 11. Na–K–$Mg^{1/2}$ triangular diagram for the collected thermal discharges. The rectangle defines the position of the cold waters.
Modified after Giggenbach, 1988.

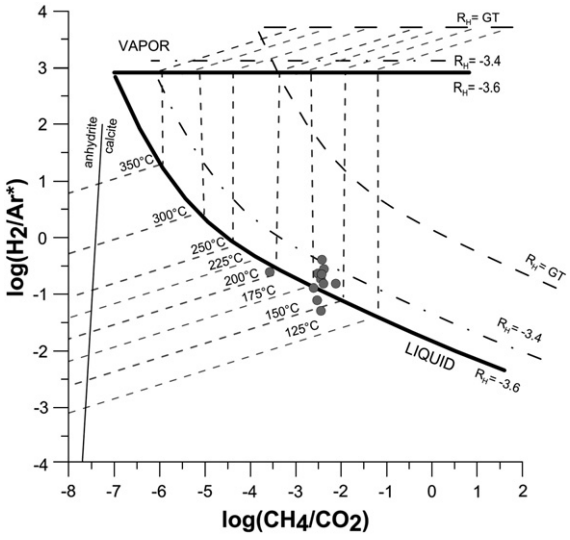

Fig. 12. $\log(H_2/Ar)$ vs. $\log(CH_4/CO_2)$ for the SVD gases. The lines shown in the diagram represent isotherms and some redox buffers usually effective in volcanic–hydrothermal environments.
Modified after Giggenbach, 1987.

fluids is likely controlled by pyrite breakdown and fayalite–hematite redox pair, as follows (Giggenbach, 1993):

$$2FeS_2 + 2FeO + 4H_2O \leftrightarrow 2FeO_{1.5} + 4H_2S \quad (10)$$

The dependence of H_2S concentrations on temperature at $R_H = -2.8$ is given by:

$$log fH_2S = 6.05 - \frac{3990}{(T-273)} \quad (11)$$

Calculations based on Eq. (11) for the SVD gases provide temperatures of 270–290 °C. Such temperatures agree with the CH_4–CO_2 geothermometer and the measured temperature of fluids from the SH2 geothermal well (290 °C) at a depth of about 2500 m (Fig. 1).

7. Gas ascent and chemistry of natural discharges: the role of the structural framework

The spatial distribution of gravity anomalies provides useful indication to evaluate the presence of carbonate structural highs in the area, being that the carbonate substratum is denser than the Neogene sedimentary rocks. As shown in Fig. 13, where the Bouguer gravity map of SVD and TM is reported, the distribution of discharges of deep-originated waters is only located at the boundary between positive and negative gravity zones, which are interpreted as extensional faults bordering buried structural highs of the carbonate basement and favoring the fluid ascent up to the surface (Chiodini et al., 1995, 1999; Pizzino et al., 2002). Conversely, the shallow-originated fluids show no relation with the tectonic assessment. Most of the fluid discharges showing significant contribution from the deep reservoir, i.e. Stigliano springs and CO_2-rich cold waters, are oriented along a NNE–SSW trend coinciding with the lithologic boundary between the SVD terrains and the sedimentary deposits of the TM (Fig. 1). The overlapping between the lithologic and the gravity limits suggests that the boundary between the volcanic and sedimentary units may represent a single structural discontinuity along which the top of the Mesozoic carbonates rise up (Barberi et al., 1994; Cimarelli and De Rita, 2006). At Stigliano, where chemistry shows clues of a significant geothermal fluid contribution, extensional faults are supposed to cut the deepest parts of the carbonate basement, where the geothermal fluid is likely confined. West of Stigliano, within the sedimentary domain of the TM, deep-originated fluids emerge only at Bagnarello and Ficoncella (samples 44 and 76), whereas the thermal and CO_2-rich waters from Tolfa, Civitavecchia and Borgo Pantani were collected from wells. This suggests that in this area the permeability of the sedimentary formations covering the carbonate basement is relatively low. All these information are reported in the schematic hydrogeological–structural section of the SVD and TM of Fig. 14, where the circulation model of fluids and the preferential pathways for their ascent to the surface is also provided.

8. Concluding remarks

The geochemical features of fluids emerging from the western sector of the SVD and the TM are mainly governed by chemical–physical processes related to gas–water–rock interactions. Waters from both shallow and deep reservoirs have a meteoric origin. In the shallow volcanic and sedimentary environments, weak water–rock interactions produce Ca(Na, K)–HCO_3 and Ca(Mg)–HCO_3 waters, respectively, whereas the main regional aquifer, which is confined within Mesozoic carbonates, has a Ca–SO_4 composition. Interaction between Ca–SO_4 fluids and a highly saline component occurs at

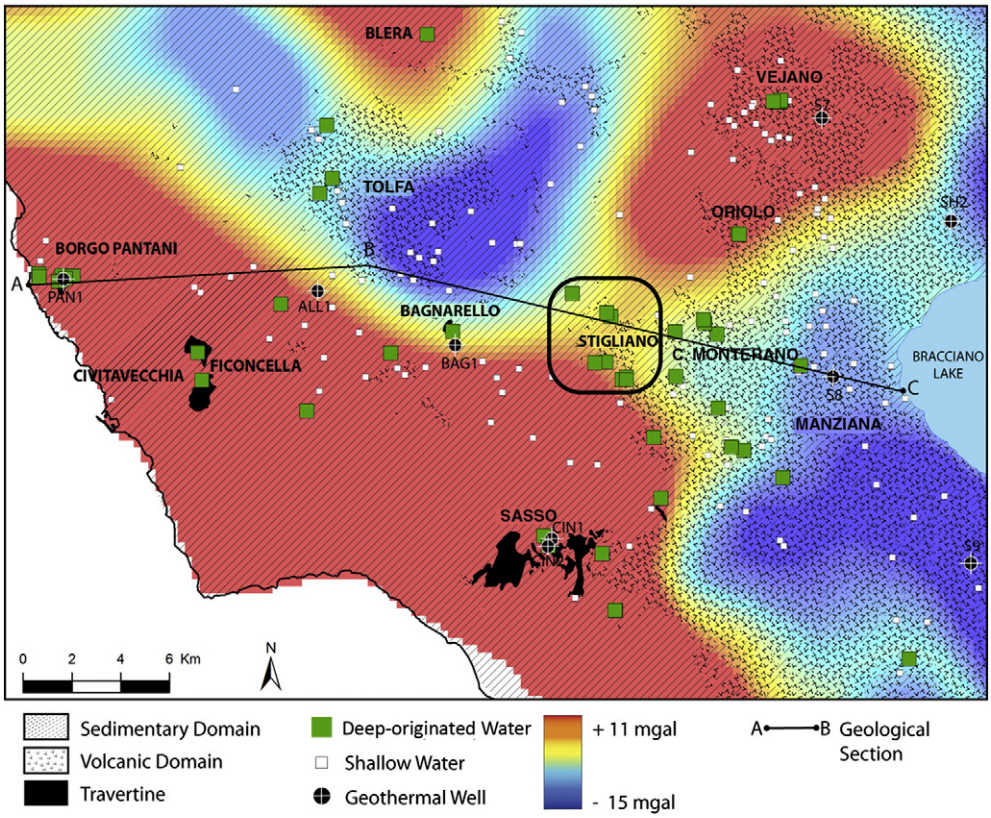

Fig. 13. Bouguer gravity map of the study area with the location of the sampling sites (waters and gases). The blue circles correspond to the deep-originated fluids (thermal waters, CO_2-rich cold waters and gas emissions). (For interpretation of the references to color in this figure legend, the reader is referred to the web version of this article.) Modified after Barberi et al., 1994.

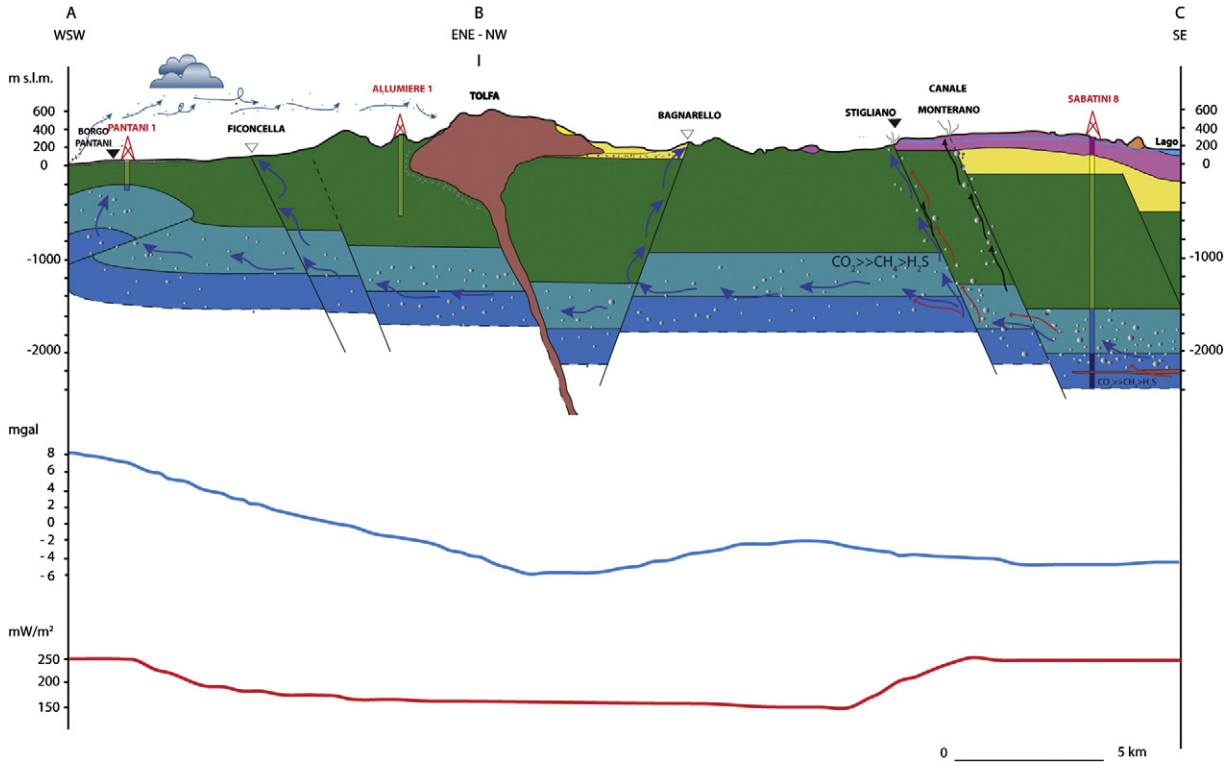

Fig. 14. Interpretative geochemical model of groundwater circulation in the western sector of the Sabatini Volcanic District and the Tolfa region. The interaction processes between shallow meteoric waters and deep fluids are shown.

Stigliano and Borgo Pantani. The high NH_4/Cl and B/Cl ratios together with the ^{18}O isotopic shift of the Stigliano fluids suggest that the Na–Cl saline deep component is likely related to the high enthalpy geothermal system of Cesano, in the eastern sector of the SVD (Calamai et al., 1976; Dall'Aglio et al., 1994).

Carbon dioxide, which is the most abundant constituent of the gas phases associated with the SVD-TM springs, is mainly produced by thermo-metamorphic reactions within the Mesozoic limestone formations and/or the underlying metamorphic basement, although significant mantle contribution cannot be ruled out. Reactions involving CO_2 and H_2 at temperatures >150 °C occurring within the carbonate reservoir are likely the main process producing CH_4. Carbon dioxide seems to play an important role even for the thermogenic production of H_2S from reduction of sedimentary sulfates at the base of the carbonate reservoir.

The spatial distribution of thermal springs, cold CO_2-rich springs and gas emissions suggests that the structural framework of the studied area, i.e. the bordering faults of buried structural highs of the carbonate basement, exerts a strong control on the uprising patterns of fluids, particularly at Stigliano, where tectonic discontinuities seem to cut the deepest parts of the carbonate basement allowing the uprising of the geothermal fluids.

Application of CH_4–CO_2 and H_2S geothermometers provide temperatures of 260–310 °C, which agree with the measured temperature of fluids from the deep geothermal wells in the SVD-TM, implying that CO_2, CH_4 and H_2S have attained chemical equilibrium within the carbonate reservoir.

Geochemical data evidence the presence of a large potential in terms of high-temperature (>200 °C) geothermal resource in the western sector of the SVD and the TM. However, utilization of the geothermal energy is at present rather poor, limited to very few installations (two spas at Stigliano and Ficoncella and a greenhouse at Borgo Pantani). The growth of demand for energy and the Kyoto Protocol directivities to reduce CO_2 emissions should encourage direct uses of geothermal energy in these areas. In the past the attempts to produce electrical generation failed mainly due to the scaling problems during the exploitation. Nevertheless, other fields of applications in the use of this alternative energy should be addressed.

Acknowledgements

Many thanks are due to two anonymous reviewers and to J. Snelleman and B. Sherwood Lollar who helped to improve an early version of the manuscript. This work was funded under Contract 1400001618 (Project leader F. Quattrocchi) and was partly supported by the "Chemical composition of free- and diffuse-gases in CO_2-rich natural analogs" project of Ciudad de la Energia (Spain) (Resp. for the CNR-IGG O. Vaselli). We thank all the municipalities and, in particular, G. Isidori for his help during the field work.

References

Abrajano, T.A., Sturchio, N.C., Bohlke, J.K., Lyon, G.L., Poreda, R.J., Stevens, C.M., 1988. Methane–hydrogen gas seeps, Zambales ophiolite, Philippines: deep or shallow origin? Chem. Geol. 7, 211–222.

Allard, P., Maiorani, A., Tedesco, D., Cortecci, G., Turi, B., 1991. Isotopic study of the origin of sulfur and carbon in Solfatara fumaroles, Campi Flegrei caldera. J. Volcanol. Geotherm. Res. 48, 139–159.

Allard, P., Jean-Baptiste, P., D'Alessandro, W., Parello, F., Parisi, B., Flehoc, C., 1997. Mantle derived helium and carbon in groundwater and gases of Mount Etna, Italy. Earth Planet. Sci. Lett. 148, 501–516.

Allegrini, G., Cappetti, G., Sabatelli, F., 1995. Geothermal development in Italy: country update report. Proc. of the World Geothermal Congress, Florence, Italy, pp. 201–208.

Anderson, R.B., 1984. The Fischer–Tropsch Synthesis. Academic Press, New York.

Arnórsson, S., Bjarnason, J.Ö., Giroud, N., Gunnarsson, I., Stefánsson, A., 2006. Sampling and analysis of geothermal fluids. Geofluids 6, 1–14.

Ault, W.U., Kulp, J.L., 1959. Isotopic geochemistry of sulphur. Geochim. Cosmochim. Acta 16, 201–235.

Baldi, P., Ferrara, G.C., Masselli, L., Pieretti, G., 1973. Hydrogeochemistry of the region between Monte Amiata and Rome. Geothermics 2, 124–141.

Ballentine, C.J., Sherwood Lollar, B., 2002. Regional groundwater focusing of nitrogen and noble gases into the Hugoton–Panhandle giant gas field, USA. Geochim. Cosmochim. Acta 66, 2483–2497.

Barberi, F., Buonasorte, G., Cioni, R., Fiordalisi, A., Foresi, L., Iaccarino, S., Laurenzi, M.A., Sbrana, A., Vernia, L., Villa, I.M., 1994. Plio-Pleistocene geological evolution of the geothermal area of Tuscany and Latium. Mem. Descr. Carta Geol. d'Italia 49, 77–134.

Barberi, F., Carapezza, M.L., Ranaldi, M., Tarchini, L., 2007. Gas blowout from shallow boreholes at Fiumicino (Rome): induced hazard and evidence of deep CO_2 degassing on the Tyrrhenian margin of central Italy. J. Volcanol. Geotherm. Res. 165, 17–31.

Barbieri, M., Masi, U., Tolomeo, L., 1979. Origin and distribution of strontium in the travertines of Latium (central Italy). Chem. Geol. 24, 181–188.

Barelli, A., Bertini, G., Buonasorte, G., Cappetti, G., Fiordelisi, A., 2000. Recent deep exploration results at the margins of the Larderello Travale geothermal system. Proc. of the World Geothermal Congress, Kyushu–Tohoku, Japan, pp. 965–970.

Bell, A.T., 1986. The mechanism of the Fischer–Tropsch synthesis. Heterogeneous Catalysis. Texas A & M University Press, College Station, TX.

Berndt, M.E., Allen, D.E., Seyfried, W.E., 1996. Reduction of CO_2 during serpentinization of olivine at 300 °C and 500 bar. Geology 24, 351–354.

Bertrami, R., Cameli, G.M., Lovari, F., Rossi, U., 1984. Discovery of Latera geothermal field: problems of the exploration and research. Seminar on Utilization of Geothermal Energy for Electric Power Production and Space Heating, Florence, pp. 1–18.

Bono, P., Capelli, G., Cattena, C., 1985. Valutazione sullo studio dell'ambiente del bacino idrografico del fiume Mignone: caratteristiche idrogeologiche. Provincia di Roma — Assessorato Ambiente, Università degli Studi "La Sapienza. Assessorato all'Ambiente ed Ecologia, Provincia di Roma.

Bréas, O., Guillou, C., Reniero, F., Wada, E., 2001. The global methane cycle: isotopes and mixing ratios, sources and sinks. Isot. Environ. Health Stud. 37, 257–379.

Buonasorte, G., Fiordalisi, A., Pandelli, E., Rossi, U., Sollevanti, F., 1987. Stratigraphic correlations and structural setting of the pre-neoautochthonous sedimentary sequences of Northern Latium. Period. Mineral. 56, 111–122.

Calamai, A., Cataldi, R., Dall'Aglio, M., Ferrara, G.C., 1976. Preliminary report on the Cesano hot brine deposit (Northern Latium, Italy). Proc. 2nd U.N. Symposium on the Development and Use of Geothermal Energy, S. Francisco, USA, pp. 305–313.

Canfield, D.E., 2001. Biogeochemistry of sulfur isotopes. Rev. Mineral. Geochem. 43, 607–636.

Capasso, G., Inguaggiato, S., 1998. A simple method for the determination of dissolved gases in natural waters. An application to thermal waters from Vulcano Island. Appl. Geochem. 13, 631–642.

Capelli, G., Mazza, R., Gazzetti, C., 2005. In: Pitagora (Ed.), Strumenti e strategie per la tutela e l'uso compatibile della risorsa idrica nel Lazio: gli acquiferi vulcanici, p. 191.

Carella, R., Verdiani, G., Palmerini, C.G., Stefani, G.C., 1985. Geothermal activity in Italy: present status and future prospects. Geothermics 14, 247–254.

Cartwright, I., Weaver, T., Tweed, S., Ahearne, D., Cooper, M., Czapnik, K., Tranter, J., 2002. Stable isotope geochemistry of cold CO_2-bearing mineral spring waters, Daylesford, Victoria, Australia: sources of gas and water and links with waning volcanism. Chem. Geol. 185, 71–91.

Cataldi, R., Rendina, M., 1973. Recent discovery of a new geothermal field: Alfina. Geothermics 2, 106–116.

Cataldi, R., Mongelli, F., Squarci, P., Taffi, L., Zito, G., Calore, C., 1995. Geothermal ranking of Italian territory. Geothermics 24, 115–129.

Cavarretta, G., Lombardi, G., 1992. Origin of sulphur in minerals and fluids from Latium (Italy): isotopic constraints. Eur. J. Mineral. 4, 1311–1329.

Cavarretta, G., Tecce, F., 1987. Contact metasomatic and hydrothermal minerals in the SH2 well, Sabatini Volcanic District, Latium, Italy. Geothermics 2, 127–145.

Ceccarelli, A., Celati, R., Grassi, S., Minissale, A., Ridolfi, A., 1987. The southern boundary area of the Larderello geothermal field. Geothermics 16, 505–516.

Cerling, T.E., Solomon, D.K., Quade, J., Bowman, J.R., 1991. On the isotopic composition of carbon in soil carbon dioxide. Geochim. Cosmochim. Acta 55, 3403–3405.

Charlou, J.L., Donval, J.P., Douville, E., Radford-Knoery, J., Fouquet, Y., Bougault, H., Jean-Baptiste, P., Stievenard, M., German, C., FLORES Cruise Scientific Party, 1997. High methane flux between 15_N and the Azores triple junction, Mid-Atlantic Ridge: hydrothermal and serpentinization processes. Eos Trans. AGU 78 (46), 83.

Chiodini, G., 1994. Temperature, pressure and redox conditions governing the composition of the cold CO_2 gases discharged in the volcanic area of North Latium (Central Italy). Appl. Geochem. 9, 287–295.

Chiodini, G., Frondini, F., Ponziani, F., 1995. Deep structures and carbon dioxide degassing in Central Italy. Geothermics 24, 81–94.

Chiodini, G., Frondini, F., Kerrick, D.M., Rogie, J., Parello, F., Peruzzi, L., Zanzari, A.R., 1999. Quantification of deep CO_2 fluxes from central Italy. Examples of carbon balance for regional aquifers and of soil diffuse degassing. Chem. Geol. 159, 205–222.

Chiodini, G., Frondini, F., Cardellini, C., Parello, F., Peruzzi, L., 2000. Rate of diffuse carbon dioxide Earth degassing estimated from carbon balance of regional aquifers: the case of central Apennine, Italy. J. Geophys. Res. 105, 8423–8434.

Cimarelli, C., De Rita, D., 2006. Relatively rapid emplacement of dome-forming magma inferred from strain analyses: the case of the acid Latian dome complexes (Central Italy). J. Volcanol. Geotherm. Res. 158, 106–116.

Cortecci, G., Reyes, E., Berti, G., Casati, P., 1981. Sulfur and oxygen isotopes in Italian marine sulfate of Permian and Triassic age. Chem. Geol. 34, 65–79.

Craig, H., 1961. Isotopic variations in meteoric waters. Science 133, 1702–1703.

Craig, H., 1963. The isotopic geochemistry of water and carbon in geothermal areas. In: Tongiorgi, E. (Ed.), Nuclear Geology on Geothermal Areas. Spoleto, CNR, (Italian Council for Research, Rome), pp. 17–54.

Cross, M.M., Manninga, D.A.C., Bottrell, S.H., Wordenc, R.H., 2004. Thermochemical sulphate reduction (TSR): experimental determination of reaction kinetics and implications of the observed reaction rates for petroleum reservoirs. Org. Geochem. 35, 393–404.

Dall'Aglio, M., Duchi, V., Minissale, A., Guerrini, A., Tremori, M., 1994. Hydrogeochemistry of the volcanic district in the Tolfa and Sabatini Mountains in central Italy. J. Hydrol. 154, 195–217.

Darling, W.G., 1998. Hydrothermal hydrocarbon gases: I. Genesis and geothermometry. Appl. Geochem. 13, 815–824.

De Rita, D., Funiciello, R., Corda, L., Sposato, A., Rossi, U., 1993. Volcanic units. In: Di Filippo, M. (Ed.), Sabatini Volcanic Complex, Quaderni de "La ricerca scientifica": CNR, 114, pp. 33–79.

Des Marais, D.J., Moore, J.G., 1984. Carbon and its isotopes in mid-oceanic basaltic glasses. Earth Planet. Sci. Lett. 69, 43–57.

Di Girolamo, P., 1978. Geotectonic setting of Miocene–Quaternary volcanism in and around eastern Tyrrhenian Sea border (Italy) as deduced by major element geochemistry. Bull. Volcanol. 42–43, 229–250.

Duchi, V., Minissale, A., 1995. Distribuzione delle manifestazioni gassose nel settore peritirrenico Tosco–Laziale e loro interazione con gli acquiferi superficiali. Boll. Soc. Geol. Ital. 114, 337–351.

Duchi, V., Minissale, A., Paolieri, M., Prati, F., Valori, A., 1992. Chemical relationship between discharging fluids in the Siena–Radicofani graben and deep fluids produced by the geothermal fields of Mt. Amiata, Torre Alfina and Latera (central Italy). Geothermics 21, 401–413.

Favara, R., Grassa, F., Ingaggiato, S., Pecoraino, G., Capasso, G., 2002. A simple method to determine the $\delta^{13}C$ content of total dissolved inorganic carbon. Geofis. Int. 41, 313–320.

Federico, C., Aiuppa, A., Allard, P., Bellomo, S., Jean-Baptiste, P., Parello, F., Valenza, M., 2002. Magma-derived gas influx and water–rock interactions in the volcanic aquifer of Mt. Vesuvius, Italy. Geochim. Cosmochim. Acta 66, 963–981.

Fiebig, J., Woodland, A.B., Spangenberg, J., Oschmann, W., 2007. Natural evidence for rapid abiogenic hydrothermal generation of CH_4. Geochim. Cosmochim. Acta 71, 3028–3039.

Fiebig, J., Woodland, A., D'Alessandro, W., Puttmann, W., 2009. Excess methane in continental hydrothermal emissions is abiogenic. Geology 37, 495–498.

Field, C., Lombardi, G., 1972. Sulfur isotopic evidence for the supergene origin of al unite deposits, Tolfa District, Italy. Miner. Deposita 7, 113–125.

Fischer, F., Tropsch, H., 1926. Die Erodo¨lsynthese bei gewo¨hnlichem druck aus den vergangsprodukten der kohlen. Brennstoff Chem. 7, 97–116.

Fischer, T.P., Giggenbach, W.F., Sano, Y., Williams, S.N., 1998. Fluxes and sources of volatiles discharged from Kudryavy, a subduction zone volcano, Kurile Islands. Earth Planet. Sci. Lett. 160, 81–96.

Foustoukos, D.I., Seyfried, W.E., 2004. Hydrocarbons in hydrothermal vent fluids: the role of chromium-bearing catalysts. Science 304, 1002–1004.

Frondini, F., 2008. Geochemistry of regional aquifer systems hosted by carbonate–evaporite formations in Umbria and southern Tuscany (central Italy). Appl. Geochem. 23, 2091–2104.

Frondini, F., Caliro, S., Cardellini, C., Chiodini, G., Morgantini, N., 2009. Carbon dioxide degassing and thermal energy release in the Monte Amiata volcanic–geothermal area (Italy). Appl. Geochem. doi:10.1016/j.apgeochem.2009.01.010.

Funiciello, R., Mariotti, G., Parotto, M., Preite-Martinez, M., Tecce, F., Toneatti, R., Turi, B., 1979. Geology, mineralogy and stable isotope geochemistry of the Cesano geothermal field (Sabatini Mountains, Northern Latium, Italy). Geothermics 8, 55–73.

Giggenbach, W.F., 1980. Geothermal gas equilibria. Geochim. Cosmochim. Acta 44, 2021–2032.

Giggenbach, W.F., 1987. Redox processis governing the chemistry of fumarolic gas discharges from White Island, New Zealand. Appl. Geochem. 2, 143–161.

Giggenbach, W.F., 1988. Isotopic and chemical assessment of geothermal potential of the Coili Albani area, Latium region, Italy. Appl. Geochem. 3, 475–486.

Giggenbach, W.F., 1991. Chemical techniques in geothermal exploration. Application of Geochemistry in Geothermal Reservoir Development. UNITAR, New York, pp. 253–273.

Giggenbach, W.F., 1992. The composition of gases in geothermal and volcanic systems as a function of tectonic setting. Proc. of the International Symposium of Water–Rock Interaction, WRI-8, pp. 873–878.

Giggenbach, W.F., 1993. Redox control of gas compositions in Philippines volcanic–hydrothermal systems. Geothermics 22, 575–587.

Giggenbach, W.F., 1997. The origin and evolution of fluids in magmatic–hydrothermal systems, In: Barnes, H.L. (Ed.), Geochemistry of Hydrothermal ore Deposits, 3 rd Edition. Wiley, pp. 737–796.

Giggenbach, W.F., Gougel, R.L., 1989. Method for the collection and analysis of geothermal and volcanic water and gas samples. NZ-DSIR Report, CD, 2387, p. 53.

Giggenbach, W.F., Matsuo, S., 1991. Evaluation of results from second and third IAVCEI workshops on volcanic gases, Mt Usu, Japan, and White Island, New Zealand. Appl. Geochem. 6, 125–141.

Grassi, S., Cortecci, G., 2005. Hydrogeology and geochemistry of the multilayered confined aquifer of the Pisa plain (Tuscany — central Italy). Appl. Geochem. 20, 41–54.

Hilton, D.R., Hammerschmidt, K., Teufel, S., Friedrichsen, H., 1993. Helium isotope characteristics of Andean geothermal fluids and lavas. Earth Planet. Sci. Lett. 120, 265–282.

Holloway, J.R., 1984. Graphite–CH_4–H_2O–CO_2 equilibria at low-grade metamorphic conditions. Geology 12, 455–458.

Holm, N.G., Charlou, J.L., 2001. Initial indications of abiotic formation of hydrocarbons in the rainbow ultramafic hydrothermal system, Mid-Atlantic ridge. Earth Planet. Sci. Lett. 191 (1–2), 1–8.

Honma, H., Itihara, Y., 1981. Distribution of ammonium in minerals of metamorphic and granitic rocks. Geochim. Cosmochim. Acta 13, 225–232.

Hooker, P.J., Bertrami, R., Lombardi, S., O'Nions, R.K., Oxburgh, E.R., 1985. Helium-3 anomalies and crust–mantle interaction in Italy. Geochim. Cosmochim. Acta 49, 2505–2513.

Horita, J., Berndt, M.E., 1999. Abiogenic methane formation and isotopic fractionation under hydrothermal conditions. Science 285, 1055–1057.

Hu, G., Ouyang, Z., Wang, X., Wen, Q., 1998. Carbon isotope fractionation in the process of Fischer–Tropsch reaction in primitive solar nebular. Sci. China, Ser. D 41, 202–207.
Hulston, J.R., Lupton, J.E., 1996. Helium isotope studies of geothermal fields in the Taupo Volcanic Zone, New Zealand. J. Volcanol. Geotherm. Res. 74, 297–321.
Hunt, J.M., 1996. Petroleum Geochemistry and Geology. W.H. Freeman and Company, New York.
Inguaggiato, S., Rizzo, A., 2004. Dissolved helium isotope ratios in ground-waters: a new technique based on gas–water re-equilibration and its application to a volcanic area. Appl. Geochem. 19, 665–673.
Inguaggiato, S., Pecoraino, G., D'Amore, F., 2000. Chemical and isotopical characterization of fluid manifestations of Ischia Island, Italy. J. Volcanol. Geotherm. Res. 99, 151–178.
Javoy, M., Pineau, F., Allegre, C.J., 1982. Carbon geodynamic cycle. Nature 300, 171–173.
Jenden, P.D., Kaplan, I.R., Poreda, R.J., Craig, H., 1988. Origin of nitrogen-rich natural gases in the California Great Valley: evidence for helium, carbon and nitrogen isotope ration. Geochim. Cosmochim. Acta 52, 851–861.
Kenney, J.K., 1995. In: Sugisaki, R., Mimura, K. (Eds.), Comment on Mantle hydrocarbons: Abiotic or Biotic: Geochim. Cosmochim. Acta, 59, pp. 3857–3858.
Kiyosu, Y., Krouse, H.R., 1990. The role of organic acid in the abiogenic reduction of sulfate and the sulfur isotope effect. Geochem. J. 24, 21–27.
Kiyosu, Y., Asada, N., Yoshida, Y., 1992. Origin of light hydrocarbon gases from the Matsukawa geothermal area in Japan. Chem. Geol. 94, 321–329.
Krouse, R.H., Viau, C.A., Eliuk, L.S., Ueda, A., Halas, S., 1988. Chemical and isotopic evidence of thermochemical sulphate reduction by light hydrocarbon gases in deep carbonate reservoirs. Nature 333, 415–419.
Kugler, E.L., Steffgen, F.W., Kugler, E.L., Steffgen, F.W., 1979. Hydrocarbon synthesis from carbon monoxide and hydrogen. Advances in Chemistry Series 178. American Chemical Society, Washington, DC.
Machel, H.G., Krouse, H.R., Sassen, R., 1995. Products and distinguishing criteria of bacterial and thermochemical sulphate reduction. Appl. Geochem. 10, 373–389.
Magro, G., Ruggieri, G., Gianelli, G., Bellani, S., 2003. Helium isotopes in paleofluids and present-day fluids of the Larderello geothermal field: constraints on the heat source. J. Geophys. Res. 108B1. doi:10.1029/2001JB001590.
Mamyrin, B.A., Tolstikhin, I.N., 1984. Helium Isotopes in Nature. Elsevier, Amsterdam.
Marini, L., Bonaria, V., Guidi, M., Hunziker, J.C., Ottonello, G., Vetuschi Zuccolini, M., 2000. Fluid geochemistry of the Acqui Terme–Visone geothermal area (Piemonte, Italy). Appl. Geochem. 15, 917–935.
Marini, L., Gambardella, B., Principe, C., Arias, A., Brombach, T., Hunziker, J.C., 2002. Characterization of magmatic sulfur in the Aegean Island arc by means of the $\delta^{34}S$ values of fumarolic H_2S, elemental S, and hydrothermal gypsum from Nysiros and Milos islands. Earth Planet. Sci. Lett. 200, 15–31.
Martelli, M., Nuccio, P.M., Stuart, F.M., Burgess, R., Ellam, R.M., Italiano, F., 2008. Helium–strontium isotope constraints on mantle evolution beneath the Roman Comagmatic Province, Italy. Earth Planet. Sci. Lett. 224, 295–308.
Marty, B., Jambon, A., 1987. $C/^3He$ in volatile fluxes from the solid Earth: implications, for carbon geodynamics. Earth Planet. Sci. Lett. 83, 16–26.
Marty, B., O'Nions, R.K., Oxburgh, E.R., Martel, D., Lombardi, S., 1992. Helium isotopes in Alpine regions. Tectonophysics 206, 71–78.
Marty, B., Trull, T., Lussiez, P., Basile, I., Tanguy, J.C., 1994. He, Ar, O, Sr and Nd isotope constraints on the origin and evolution of Mount Etna magmatism. Earth Planet. Sci. Lett. 126, 23–39.
McCollom, T.M., 2003. Formation of meteorite hydrocarbons from thermal decomposition of siderite ($FeCO_3$). Geochim. Cosmochim. Acta 67, 311–317.
McCollom, T.M., Seewald, J.S., 2007. Abiotic synthesis of organic compounds in deep-sea hydrothermal environments. Chem. Rev. 107, 382–401.
Mingram, B., Brauer, K., 2001. Ammonium concentration and nitrogen isotope composition in metasedimentary rocks from different tectonometamorphic units of the European Variscan Belt. Geochim. Cosmochim. Acta 65, 273–288.
Minissale, A., 2004. Origin, transport and discharge of CO_2 in Central Italy. Earth Sci. Rev. 66, 89–141.
Minissale, A., Duchi, V., 1988. Geothermometry on fluids circulating in a carbonate reservoir in north-central Italy. J. Volcanol. Geotherm. Res. 35, 237–252.
Minissale, A., Evans, W., Magro, G., Vaselli, O., 1997a. Multiple source components in gas manifestations from north-central Italy. Chem. Geol. 142, 175–192.
Minissale, A., Magro, G., Vaselli, O., Verrucchi, C., Perticone, I., 1997b. Geochemistry of water and gas discharges from the Mt. Amiata silicic complex and surrounding areas (central Italy). J. Volcanol. Geotherm. Res. 79, 223–251.
Minissale, A., Kerrick, D.M., Magro, G., Murrell, M.T., Paladini, M., Rihs, S., Sturchio, N.C., Tassi, F., Vaselli, O., 2002. Geochemistry of Quaternary travertines in the region north of Rome (Italy): structural, hydrologic and paleoclimatic implications. Earth Planet. Sci. Lett. 203, 709–728.
Montegrossi, G., Tassi, F., Vaselli, O., Buccianti, A., Garofano, K., 2001. Sulfur species in volcanic gases. Anal. Chem. 73, 3709–3715.
Negrel, P., Casanova, J., Azaroual, M., Guerrot, C., Cocherie, A., Fouillac, C., 1999. Isotope geochemistry of mineral spring waters in the Massif Central France. In: Armannsson, H. (Ed.), Geochemistry of Earth's Surface. Rotterdam, The Netherlands.
Ohmoto, H., Lasaga, A.C., 1982. Kinetics of reactions between aqueous sulphates and sulphides in hydrothermal system. Geochim. Cosmochim. Acta 46, 1727–1745.
Ohmoto, H., Rye, R.O., 1979. Isotopes of sulfur and carbon, In: Barnes, H.L. (Ed.), Geochemistry of Hydrothermal Ore Deposits, 2nd edition. Wiley and Sons Ltd, Chichester, pp. 509–567.
Oremland, R.S., Miller, L.G., Whiticar, M.J., 1987. Sources and flux of natural gases from Mono Lake, California. Geochim. Cosmochim. Acta 51, 2915–2929.
Parkhurst, D.L., Appelo, A.A.J., 1999. User's guide to PHREEQC (version 2) — a computer program for speciation, batch-reaction, one dimensional transport and inverse geochemical modeling. U.S.G.S. Water Res. Inv. Rep. 99–4259, 312.
Peccerillo, A., 1999. Multiple mantle metasomatism in central–southern Italy: geochemical effects, timing and geodynamic implications. Geology 27, 315–318.
Peccerillo, A., Poli, G., Tolomeo, L., 1984. Genesis, evolution and tectonic significance of K-rich volcanics from the Alban Hills (Roman Comagmatic Region) as inferred from trace element geochemistry. Contrib. Mineral. Petrol. 86, 230–240.
Pizzino, L., Galli, G., Mancini, C., Quattrocchi, F., Scarlato, P., 2002. Natural gas hazard (CO_2, ^{222}Rn) within a quiescent volcanic region and its relations with tectonics: the case of the Ciampino–Marino area, Alban Hills Volcano. Italy. Nat. Hazards 27, 257–287.
Poreda, R.J., Craig, H., 1989. Helium isotope ratios in circum-Pacific volcanic arcs. Nature 338, 473–478.
Poreda, R.J., Jeffrey, A.W.A., Kaplan, L.R., Craig, H., 1988. Magmatic helium in subduction-zone natural gases. Chem. Geol. 71, 199–210.
Rice, D.D., Claypool, G.E., 1981. Generation, accumulation, and resource potential of biogenic gas. AAPG Bull. 65, 5–25.
Risacher, F., Alonso, H., Salazar, C., 2002. Hydrochemistry of two adjacent acid saline lakes in the Andes of northern Chile. Chem. Geol. 187, 39–57.
Rollinson, H., 1993. Using Geochemical Data. Longman Group, London.
Rowe, G.L., 1994. Oxygen, hydrogen, and sulfur isotope systematic of the crater lake system of Poás Volcano, Costa Rica. Geochem. J. 28, 263–287.
Rye, R.O., Bethke, P.M., Wasserman, M.D., 1992. The stable isotope geochemistry of acid sulfate alteration. Econ. Geol. 87, 225–262.
Sakai, H., 1968. Isotopic properties of sulfur compounds in hydrothermal processes. Geochim. J. 2, 29–49.
Sano, Y., Marty, B., 1995. Origin of carbon in fumarolic gas from island arcs. Chem. Geol. 119, 265–274.
Schoell, M., 1980. The hydrogen and carbon isotopic composition of methane from natural gases of various origins. Geochim. Cosmochim. Acta 44, 649–661.
Schoell, M., 1988. Multiple origins of methane in the Earth. Chem. Geol. 71, 1–10.
Sepulveda, F., Lahsen, A., Powell, T., 2007. Gas geochemistry of the Cordón Caulle geothermal system, Southern Chile. Geothermics 36, 389–420.
Shaw, D.M., Sturchio, N.C., 1992. Boron–lithium relationships in rhyolites and associated thermal waters of young silicic calderas, with comments on incompatible element behaviour. Geochim. Cosmochim. Acta 56, 3723–3731.
Sherwood Lollar, B., Westgate, T.D., Ward, J.A., Slater, G.F., Lacrampe-Couloume, G., 2002. Abiogenic formation of alkanes in the Earth's crust as a minor source for global hydrocarbon reservoirs. Nature 416, 522–524.
Shock, E.L., 1993. Hydrothermal dehydration of aqueous organic compounds. Geochim. Cosmochim. Acta 57, 3341–3349.
Snyder, G., Poreda, R.J., Fehn, U., Hunt, A., 2003. Sources of nitrogen and methane in Central American geothermal settings: Noble gas and ^{129}I evidence for crustal and magmatic volatile components. Geochem. Geophys. Geosys. doi:10.1029/2002GC000363.
Sugisaki, R., Mimura, K., 1994. Mantle hydrocarbons: abiotic or biotic? Geochim. Cosmochim. Acta 58, 2527–2542.
Szatmari, P., 1989. Petroleum formation by Fischer–Tropsch synthesis in plate tectonics. AAPG Bull. 73, 989–998.
Taran, Y., Fisher, T.P., Cienfuegos, E., Morales, P., 2002. Geochemistry of hydrothermal fluids from an intraplate ocean island: Everman volcano, Socorro Island, Mexico. Chem. Geol. 188, 51–63.
Tedesco, D., Scarsi, P., 1999. Intensive gas sampling of noble gases and carbon at Vulcano Island (southern Italy). J. Geophys. Res. 104-B5, 10499–10510.
Tedesco, D., Allard, P., Sano, Y., Wakita, H., Pece, R., 1990. Helium-3 in subaerial and submarine fumaroles of Campi Flegrei caldera, Italy. Geochim. Cosmochim. Acta 54, 1105–1116.
Thode, H.G., 1991. Sulphur isotope in nature and the environment: an overview. In: Krouse, H.R., Grinenko, V.A. (Eds.), Stable Isotopes — Natural and Anthropogenic Sulphur in the Environment. : Scope, 43. Wiley, Chichester, pp. 1–23.
Vaselli, O., Tassi, F., Montegrossi, G., Capaccioni, B., Giannini, L., 2006. Sampling and analysis of volcanic gases. Acta Volcanol. 18, 65–76.
Verma, S., Santoyo, E., 1997. New improved equations for Na/K, Na/Li and SiO_2 geothermometers by outlier detection and rejection. J. Volcanol. Geotherm. Res. 79, 9–23.
Welhan, J.A., Craig, H., 1979. Methane and hydrogen in East Pacific Rise hydrothermal fluids. Geophys. Res. Lett. 6, 829–831.
Welhan, J.A., Poreda, R.J., Rison, W., Craig, H., 1988. Helium isotopes in geothermal and volcanic gases of the western United States. I. Regional variability and magmatic origin. J. Volcanol. Geotherm. Res. 34, 185–199.
Whitfield, M., 1978. Activity coefficients in natural waters. In: Pytkowicz, R.M. (Ed.), Activity Coefficients in Electrolyte Solutions. CRC Press, Boca Raton, FL, pp. 153–300.
Whiticar, M.J., 1999. Carbon and hydrogen isotope systematics of bacterial formation and oxidation of methane. Chem. Geol. 161, 291–314.
Whiticar, M.J., Suess, E., 1990. Hydrothermal hydrocarbon gases in the sediments of the King-George Basin, Bransfield Strait, Antarctica. Appl. Geochem. 5, 135–147.
Worden, R.H., Smalley, P.C., 1996. H_2S-producing reactions in deep carbonate gas reservoirs: Khuff Formation, Abu Dhabi. Chem. Geol. 133, 157–171.
Wynn, J.G., Sumrall, J.B., Onac, B.P., 2010. Sulfur isotopic composition and the source of dissolved sulphur species in thermo-mineral springs of the Cerna Valley, Romania. Chem. Geol. 271, 31–43.
Yuen, G.U., Pecore, J.A., Kerridge, J.F., Pinnavaia, T.J., Rightor, E.G., Flores, J., Wedeking, R., Des Marais, D.J., Chang, S., 1990. Carbon isotope fractionation in the Fischer–Tropsch type reactions. Lunar and Planetary Science Conference Proc. XXI, Houston, Texas, pp. 1367–1368.
Zhang, J., Quay, P.D., Wilbur, D.O., 1995. Carbon isotope fractionation during gas–water exchange and dissolution of CO_2. Geochim. Cosmochim. Acta 82, 161–173.
Zuppi, G.M., Fontes, J.C., Letolle, R., 1974. Isotopes du milieu et circulation d'eaux sulfurées dans le Latium. Isotope Techniques in Groundwater Hydrology, 1. IAEA, Vienna, pp. 341–361.